Available online at www.sciencedirect.com

ScienceDirect

Geochimica et Cosmochimica Acta 269 (2020) 465–483

Geochimica et Cosmochimica Acta

www.elsevier.com/locate/gca

Neodymium isotopes track sources of rare earth elements in acidic mine waters

Irene L.R. Wallrich [1], Brian W. Stewart *, Rosemary C. Capo, Benjamin C. Hedin, Thai T. Phan [2]

Department of Geology & Environmental Science, University of Pittsburgh, Pittsburgh, PA 15260, USA

Received 22 February 2019; accepted in revised form 30 October 2019; available online 7 November 2019

Abstract

Acid mine drainage (AMD) has been proposed as a potential source of strategic rare earth elements (REEs) due to its high concentrations (>1000 μg/L) of dissolved REEs, as well as the middle rare earth element (MREE) enriched pattern exhibited by both coal mine- and metal mine-derived AMD, in which some of the most energy-critical REEs are significantly concentrated. However, the source of REEs and the origin of the MREE enrichment observed in AMD discharges is poorly understood; suggestions include dissolution of MREE-enriched surface coatings, fractionation by colloids, solid-liquid exchange reactions, incongruent dissolution of pyrite, and selective leaching of MREE-enriched phases. Filtration experiments on acidic to circumneutral AMD (unfiltered to <0.002 μm) indicate that REEs are in a dissolved state. Thus, colloids are not a significant carrier of REEs in these samples and are not responsible for the observed MREE-enriched patterns. The similarity of MREE-enriched patterns exhibited by AMD to those of laboratory sulfuric acid (simulated AMD) leachates of corresponding overburden samples suggest that these lithologies are a major contributor of REEs to AMD. Isotopes of strontium ($^{87}Sr/^{86}Sr$) and neodymium ($^{143}Nd/^{144}Nd$) in AMD discharges are distinct from whole-rock values of associated lithologies, but fall within the range of values of the leachates. Whole rocks, leachates, and AMD define a trend on a Sm-Nd isochron diagram consistent with the ~310 Ma depositional age of the coal. These data suggest that MREE enrichment of AMD results from preferential leaching of a readily dissolvable, MREE-enriched mineral phase, most likely apatite or a related phosphate phase, that formed during or shortly after deposition of the coal and associated units.

Keywords: Rare earth elements; REE; Coal mine; AMD; Nd isotopes; Sr isotopes; Apatite

1. INTRODUCTION

Discharges from surface and underground metal and coal mines can transport significant quantities of metals and acidity into streams and groundwater. These loadings result from the oxidation of sulfide minerals (usually pyrite, FeS_2, in coal mines) when exposed to oxygen and water, according to the following overall reaction (Nordstrom and Alpers, 1999; Johnson and Hallberg, 2005; Akcil and Koldas, 2006; Blowes et al., 2014; Simate and Ndlovu, 2014; Nordstrom et al., 2015):

$$FeS_2 + 15/4\ O_2 + 7/2\ H_2O \rightarrow Fe(OH)_3(s) + 2\ SO_4^{2-} + 4H^+ \quad (1)$$

Reaction (1) summarizes a three-step oxidation process where both sulfur and ferrous iron in pyrite are oxidized

* Corresponding author.
E-mail address: bstewart@pitt.edu (B.W. Stewart).
[1] Present address: Vanderbilt University Graduate School, Vanderbilt University, Nashville, TN 37240, USA.
[2] Present address: Department of Earth and Environmental Sciences, University of Waterloo, 200 University Ave. W, Waterloo, Ontario, Canada.

https://doi.org/10.1016/j.gca.2019.10.044
0016-7037/

and ferric iron is hydrolyzed. Several chemical (*e.g.*, Fe^{3+} reactivity, site mineralogy, pH, Eh), physical (*e.g.,* temperatures, surface area, permeability), and biological (*e.g.,* microbial populations) factors determine the rate of these reactions at a given site (Nordstrom and Alpers, 1999; Plumlee et al., 1999; Akcil and Koldas, 2006; Nordstrom, 2011; Blowes et al., 2014; Nordstrom et al., 2015). The acid generated by these reactions dissolves minerals along the groundwater flow path, which results in elevated concentrations of Al, Mn, and heavy metals in mine drainage (Akcil and Koldas, 2006; Cravotta, 2008a), in addition to elevated concentrations of dissolved or particulate iron from pyrite oxidation. Flows of acidic, metal-polluted waters can continue for decades after operations have ceased, degrading water quality, reducing aquatic diversity, and corroding infrastructure (Younger, 1997; Johnson and Hallberg, 2005; Cravotta, 2008a; Jennings et al., 2008; Simate and Ndlovu, 2014). Acid mine drainage (AMD) is a global problem (Li et al., 2008), both for countries with under-regulated to non-regulated mining industries operating today, and for regions with historic mines that operated with little to no regulation. The Appalachian Basin is an example of the latter, with extensive coal resources and a long mining history. It is estimated that in Pennsylvania alone, over 4500 km of waterways have been affected by AMD (USGS, 2010).

In addition to metals, AMD can contain elevated concentrations of rare earth elements (REEs) (Cravotta, 2008a; 2008b; Ayora et al., 2016; Stewart et al., 2017), here defined as the lanthanides (atomic numbers 57 to 71) and yttrium (Y). Rare earth elements have unique chemical and physical properties that result from filling of the f-orbital, leading to a systematic decrease in ionic radius with increasing atomic number. These properties, along with their high (3+) valence, can allow for the retention of source signatures through weathering, deposition, and diagenesis, making REEs powerful tracers for clastic sediment transport (McLennan, 1989). In some cases, fluid-rock interactions in aqueous environments can affect the relative concentrations of the REEs, leaving characteristic signatures in both the fluids and the solid residues (Elderfield et al., 1990; Bau and Möller, 1993; Johannesson and Zhou, 1999; Worrall and Pearson, 2001). The unique chemical and physical properties of REEs have also made them essential components of lamp phosphors, catalysts, and electronics, notably permanent magnets and rechargeable batteries (Binnemans et al., 2013; Wall, 2014). Due to concerns with global market supply and increasing demand for REEs in growing technological sectors such as renewable energy, the search for alternative sources of REEs (notably: Nd, Dy, Tb, Eu, Yb) has become a growing priority for many countries (DOE, 2011; Binnemans et al., 2013; European Commission, 2014). Recent demand for alternative sources of Nd and other strategic REEs has resulted in several studies investigating the feasibility of economic recovery of REEs from coal deposits and coal by-products like AMD and coal fly ash (Seredin and Dai, 2012; Ayora et al., 2016; Franus et al., 2015; Ziemkiewicz et al., 2016; Stewart et al., 2017; Hedin et al., 2019; Vass et al., 2019).

When normalized to a shale composition, REE patterns in AMD commonly show enrichment in the middle rare earth elements (MREEs; Sm to Dy), distinct from the whole-rock REE patterns of the lithologies with which the AMD interacts. This MREE-enriched pattern has been observed in a wide range of natural and anthropogenic low-pH systems (Johannesson et al., 1996; Worrall and Pearson, 2001; Åström and Corin, 2003; Merten et al., 2005; Olías et al., 2005; Zhao et al., 2007; Pérez-López et al., 2010; Stewart et al., 2017). However, the source of REEs and the MREE-enrichment found in mine drainage and other acidic waters remains uncertain. The concentrations of REEs in rainwater are too low (e.g., Sholkovitz et al., 1993; Iwashita et al., 2011) to significantly affect the patterns and abundances in AMD, so the REE must be derived from water-rock interaction. Several studies have proposed various source- and process-driven controls for this enrichment pattern, including preferential leaching of a MREE-enriched mineral phase in local strata (Worrall and Pearson, 2001; Merten et al., 2005; Leybourne and Cousens, 2005; Sun et al., 2012); MREE mobilization by S-species complexation during pyrite oxidation (Grawunder et al., 2014); fractionation by colloidal complexes (Åström and Corin, 2003); solid-liquid exchange reactions with surface coatings and/or clays (Gimeno Serrano et al., 2000; Leybourne et al., 2000; Åström, 2001; Coppin et al., 2002; Gammons et al., 2005); preferential removal of light and heavy REEs via the formation of secondary minerals (Welch et al., 2009); and differences in aqueous complexation for different REEs (Möller and Bau, 1993; Sholkovitz, 1995; Dia et al., 2000; Tang and Johannesson, 2003; Zhao et al., 2007). However, the evaluation of REE patterns alone yields non-unique solutions to the problem of MREE enrichment in mine drainage.

To understand AMD-rock interactions and determine the source of strategic REEs, we conducted experiments using simulated AMD in a well-constrained coal mine discharge system. Radiogenic strontium (Sr) and neodymium (Nd) isotope compositions from these experiments were then compared with those of coal mine drainage collected in the field. Strontium isotopes can be used to quantitatively track water-rock interaction, particularly the source and fate of alkaline earth elements like Ca, because the $^{87}Sr/^{86}Sr$ ratio, which varies as a result of ^{87}Rb decay, differs in different lithologies and is not significantly affected by mass-dependent isotope fractionation (Capo et al., 1998; Stewart et al., 1998; Banner, 2004). Due to the similar chemical and physical properties that the REEs share, the source and transport behavior of Nd should be an ideal proxy for the behavior of REEs as a whole. The alpha decay of ^{147}Sm (half-life $= 1.06 \times 10^{11}$ yr) produces ^{143}Nd, resulting in rocks and minerals developing unique $^{143}Nd/^{144}Nd$ ratios over millions to billions of years. This allows the $^{143}Nd/^{144}Nd$ ratio to be used as a tracer for the origin of Nd, and by extension other REEs, in ground and surface waters interacting with those rocks and minerals. In particular, use of this isotope system can help differentiate between sources or processes associated with deposition and diagenesis of the sediments, and recent

processes related to the generation of AMD. Constraining the origin of REEs in AMD will increase our understanding of water-rock reactions and the long-term evolution of natural and anthropogenic low-pH groundwater systems. It will also provide predictive capability and resource assessment for potential new REE sources resulting from acidic water-rock interaction.

2. MATERIALS AND METHODS

2.1. Solid samples and leachates

Rock samples for this study were collected in western Pennsylvania, at the Pittsburgh Botanic Gardens (PBG; Fig. 1). In 2011, as part of an ongoing reclamation project, the PBG authorized the surface mining of an abandoned Pittsburgh Coal room-and-pillar mine (Czebiniak, 2016). The abandoned deep-mine, which operated in the early 1900s, was a gravity drained, unflooded mine that produced untreated AMD. Subsequent surface mining allowed for the sampling of a representative stratigraphic section of the lower Pittsburgh Formation, including the underclay (which represents the mine floor beneath the main coal seam), main Pittsburgh Coal seam, clay partings, roof coal, clastic overburden units, and mineral separates of pyrite from the main coal seam (Fig. 2). Samples within ~2 m of the base of the Pittsburgh coal were collected from unmined pillars, and samples from above this zone were collected from undisturbed strata overlying the abandoned mine portals. All samples were collected from fresh surfaces exposed by strip mining and showed no evidence of previous water infiltration, and no visible evidence of iron oxidation on sample surfaces or fractures. Pyrite nodules from relatively unweathered samples of the Pittsburgh Coal main seam (PA-PBG-1) were coarsely crushed and manually separated from the coal samples. Pyrite was then finely crushed and separated from organic matter using a bromoform heavy liquid density separation. Dried pyrite separates were split and analyzed for elemental composition.

Whole-rock samples were powdered in a tungsten-carbide ball mill and split for analysis. One split was reserved for major and trace element analysis. A second split (~2 g) was sequentially leached with ultrapure reagents. Samples were leached for 4 h with 1 N ammonium acetate (NH_4Ac), buffered to a pH of 8, to remove easily exchangeable ions (Stewart et al., 2001). The residues were rinsed with ultrapure (Milli-Q, 18.2 MΩ) water, and then leached with 0.05 M sulfuric acid (pH=1.3; prepared using

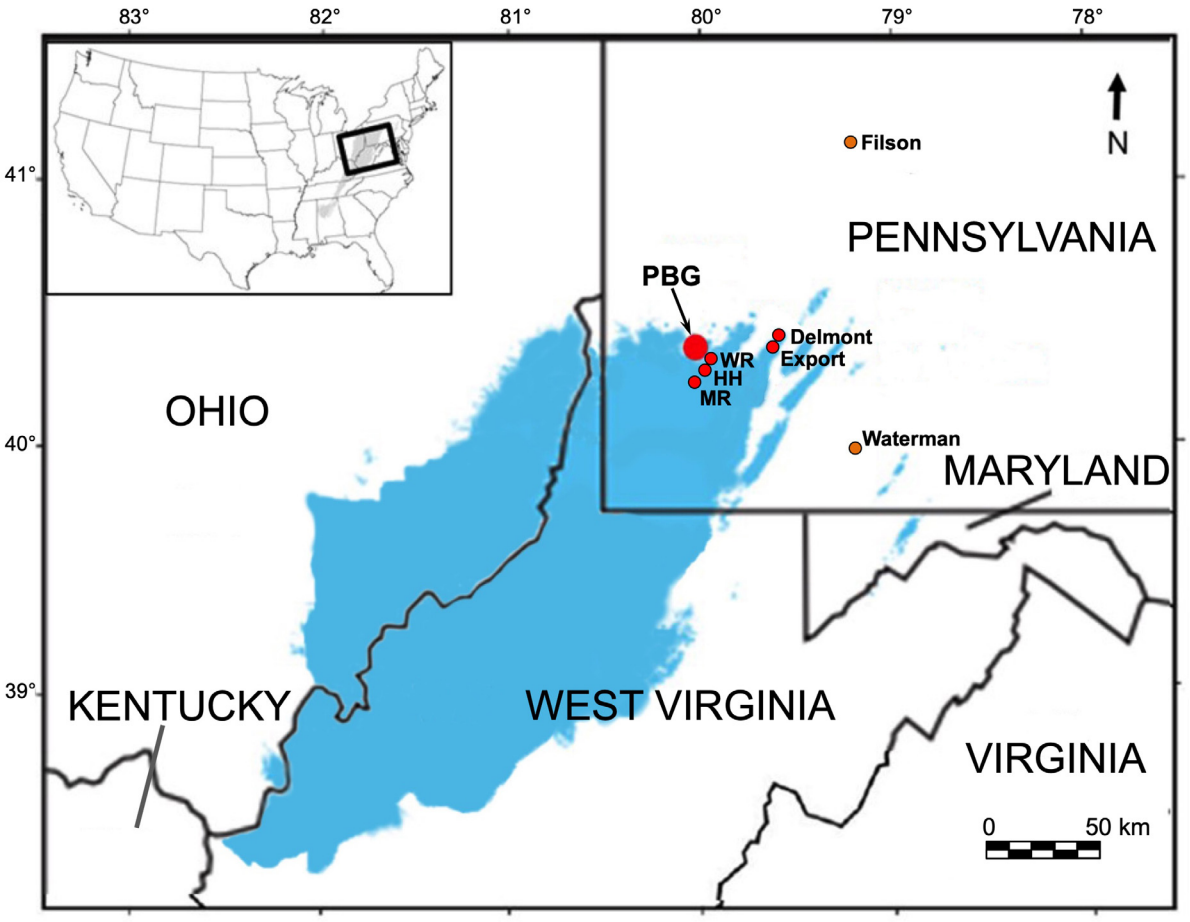

Fig. 1. Map of the study area, showing the extent of the Pittsburgh Coal bed (shaded in blue; modified from Ruppert et al., 2002). PBG is the Pittsburgh Botanic Garden field site; additional discharges from the Pittsburgh Coal are shown in red (Delmont, Export, WR = Whiskey Run, HH = Hope Hollow, MR = McLaughlin Run), while the Filson and Waterman sites are discharges from underlying coal units.

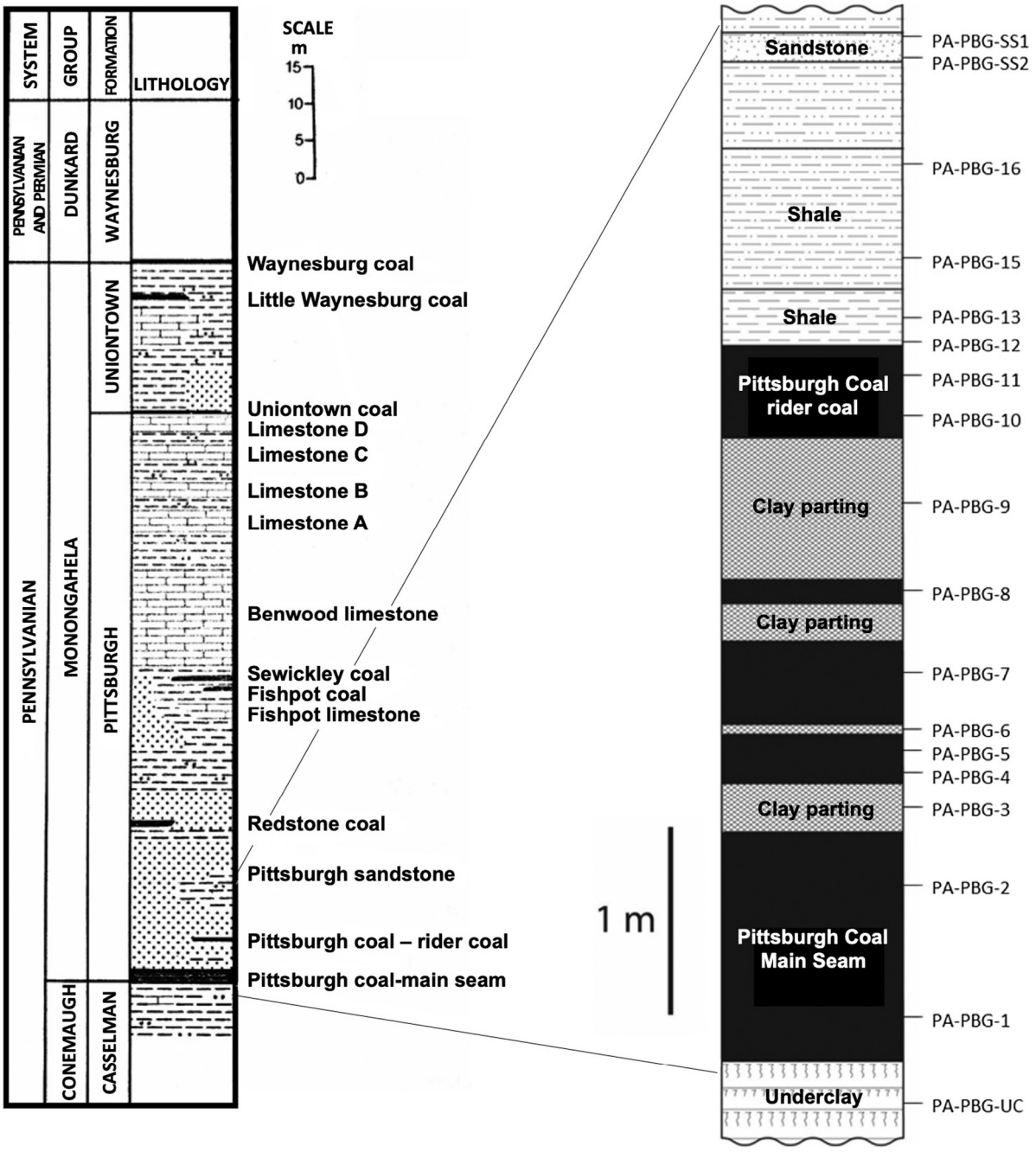

Fig. 2. Left: cross section of Pennsylvanian coal-bearing units in western Pennsylvania (from Edmunds et al., 1999). Right: stratigraphy of sampled strip mine and sample locations, based on field measurements.

Optima® ultrapure H_2SO_4) for 4 h to simulate the effects of AMD. The liquid:sample ratio (mass/mass) for all leaching experiments was 40:1, and all leachates were filtered to <0.2 μm using acid-cleaned Nalgene® cellulose acetate filter cartridges on a FisherBrand Luer-Lok® syringe.

2.2. Acid mine drainage samples

Acid mine drainage samples (60–120 mL) were collected for geochemical analysis in December 2016 from an underground pipe from the Pittsburgh Coal deep mine on the PBG property (approximately 800 m northwest of the surface mine sampling site) that feeds into the PBG passive treatment system installed by Hedin Environmental, Inc. All samples were filtered to <0.45 μm using an acid-cleaned 60 mL FisherBrand Luer-Lok® syringe with acid-cleaned SFDA-membrane filter cartridges (Cole-Parmer) in acid-washed polypropylene bottles and acidified with ultrapure nitric acid (HNO_3) to a pH < 2.0. Field measurements of

AMD included pH, temperature, conductivity, and alkalinity.

Mine drainage with a range of pH values (3.2–6.4; Table S4) was collected for filtration experiments to investigate potential colloidal controls (Phan et al., 2018b) on REE chemistry. Samples were collected from PBG and from four other Pittsburgh Coal mine drainage sites (Fig. 1), including two within the Irwin Syncline Basin (Winters and Capo, 2004) in April and May of 2017. Samples were filtered in the field, one to <0.45 μm (as described above) and one to <0.2 μm (using acid cleaned Nalgene® cellulose acetate filter cartridges). At each site, two additional unfiltered samples were collected with no headspace, one for analysis as-is and the other centrifuged through a 3 kDa molecular weight cut-off (MWCO) membrane filter (EMD Millipore), equivalent to ~0.002 μm, in the lab at the University of Pittsburgh within 3 h of collection. Subsequent to filtration, all filtrates were acidified with ultrapure HNO_3 to a pH < 2.0; filter retentates were not analyzed. At the PBG site, two additional replicate samples were collected for each level of filtration (unfiltered, <0.45 μm, <0.2 μm, 3 kDa).

Here we also report additional data from AMD discharges from the Pittsburgh coal seam (n = 6) and one each from discharges from the underlying Clarion and Freeport coal seams, collected between June 1999 and March 2002. These samples were filtered to <0.45 μm in the field with acid-cleaned SFDA-membrane filter cartridges and acidified as described above.

2.3. Elemental and isotopic analysis

Concentrations of major and trace elements (including REEs) in whole-rock and pyrite samples collected from PBG were determined by ICP-MS, at Activation Laboratories (ActLabs), Canada. In addition, sulfur speciation analysis and proximate analysis (moisture, ash, volatile matter, fixed C) were conducted on coal samples at ActLabs. Ash content was calculated as the residue remaining after moisture, volatiles and fixed carbon have been driven from the sample. Whole-rock major and trace element data are reported in Supplementary Information (Tables S1–S3). Rare earth element concentrations in AMD samples collected between 1999 and 2002 were determined by ICP-MS at ActLabs; these data were reported by Stewart et al. (2017), and they are used to calculate the $^{147}Sm/^{144}Nd$ of these samples (see below).

Ammonium acetate leachates, sulfuric acid leachates, and AMD from the PBG site (collected in 2016) were analyzed for 36 elements, including major elements, trace metals and Si, by ICP-OES at ActLabs. Both the leachate solutions and the AMD filtrates collected in 2016 and 2017 were analyzed for REEs on a Perkin-Elmer 300X ICP-MS under kinetic energy discrimination mode at the University of Pittsburgh, following the method described in Phan et al. (2018a). The accuracy of REE concentration data was better than ±10% based on repeated measurements of a reference water sample (USGS T227).

Neodymium and Sr isotope preparation and analysis were carried out under clean laboratory conditions at the University of Pittsburgh. Powdered whole-rock samples containing approximately 150 ng of Nd were acid digested using $HF + HNO_3 + HClO_4$, and evaporated to dryness in Teflon vials under HEPA filtered airflow. Aliquots of leachate and AMD samples containing approximately 150 ng of Nd were also evaporated to dryness in Teflon vials. Sulfuric acid leachates were treated with hydrogen peroxide when dried down due to the hydrophilic nature of the samples that was attributed to the formation of organosulfides. All samples were then re-dissolved in 1.5 N HCl.

Rare earth elements and Sr were separated from the matrix in whole-rock, leachate, and AMD samples (including those collected in 1999–2002) using cation exchange columns eluted with 1.5, 2.5 and 4.0 N HCl. Strontium isotope ratios from the 1999–2002 AMD samples are reported in Chapman et al. (2012); for all other samples, the Sr cut was further cleaned using Sr Resin® (Eichrom) following the method of Wall et al. (2013), and Sr isotope ratios were measured on a Thermo Neptune Plus® MC-ICP-MS at the University of Pittsburgh. Mass fractionation was corrected using an exponential law with $^{86}Sr/^{88}Sr = 0.1194$, and multiple measurements of the NIST SRM 987 Sr standard were interspersed throughout the sample analyses. All sample $^{87}Sr/^{86}Sr$ values were adjusted to match SRM 987 = 0.710240, the long-term value at the University of Pittsburgh lab (Capo et al., 2014). Estimated external reproducibility of the measured $^{87}Sr/^{86}Sr$ ratio is ±0.00002. Nd was separated from other REEs using columns packed with LnSpec® (Eichrom) chromatographic material (e.g., Pin and Zalduegui, 1997), eluted with 0.18 N HCl. An aliquot of approximately 150 ng of Nd was loaded onto a Re double filament assembly. Nd isotopes of the sample, as well as the La Jolla Nd Standard, were measured using a Finnigan MAT 262 multi-collector thermal ionization mass spectrometer (TIMS) at the University of Pittsburgh (Cole and Stewart, 2009). A total of 100 ratios were measured during each analysis, and mass fractionation was corrected using an exponential law, normalizing to $^{146}Nd/^{144}Nd = 0.724134$ (Wasserburg et al., 1981). Because age-corrected $^{143}Nd/^{144}Nd$ values can provide additional information about the origin of minerals contributing to AMD chemistry (see Section 4.2.2), Nd isotope data are reported as $\varepsilon_{Nd}(T)$ where

$$\in_{Nd}(T) = \left(\frac{^{143}Nd/^{144}Nd(T)_{sample}}{^{143}Nd/^{144}Nd(T)_{CHUR}} - 1 \right) 10^4$$

and T is the age of the sample and CHUR is the chondritic uniform reservoir. Our value for $^{143}Nd/^{144}Nd(0)_{CHUR}$, based on repeated analyses of the La Jolla Nd standard, is 0.511847. $^{143}Nd/^{144}Nd$ (T) is calculated from the measured ratio and the sample $^{147}Sm/^{144}Nd$ as $^{143}Nd/^{144}Nd(T) = {}^{143}Nd/^{144}Nd(0) - {}^{147}Sm/^{144}Nd(e^{\lambda T} - 1)$, where λ is the decay constant for ^{147}Sm (6.54×10^{-12} yr^{-1}) and $^{147}Sm/^{144}Nd_{CHUR}$ (used to calculate CHUR value at time T) is 0.1967 (Jacobsen and Wasserburg, 1980). $^{147}Sm/^{144}Nd$ ratios for all samples are calculated from ICP-MS REE data. The total blanks for Sr and Nd were <1% of the total analyzed sample (in most cases <0.01%); thus no blank corrections were warranted.

3. RESULTS

3.1. Acid mine drainage filtration experiments

Rare earth element data from Pittsburgh Botanic Garden AMD and other discharges from the Pittsburgh Coal (Table S4) yield MREE-enriched patterns when normalized to the North American Shale Composite (NASC; Fig. 3), consistent with previous data from Appalachian Basin coal mine drainage (Cravotta, 2008b; Cravotta and Brady, 2015; Stewart et al., 2017), as well as other coal and mineral mine drainage sites (Worrall and Pearson, 2001; Merten et al., 2005; Wood et al., 2005; Zhao et al., 2007; Pérez-López et al., 2010; Sun et al., 2012; Sahoo et al., 2012; Zhang and Honaker, 2018). In addition, REE concentrations show a clear relationship with pH, with low-pH mine drainage having the highest REE concentrations (Stewart et al., 2017), while maintaining the MREE-enriched pattern (Fig. 3). Acid mine drainage samples from this study that were filtered down to a level of ~3000 Da (~0.002 μm) show no significant difference in REE pattern or abundance relative to unfiltered waters, from a pH range of 3.2–5.1.

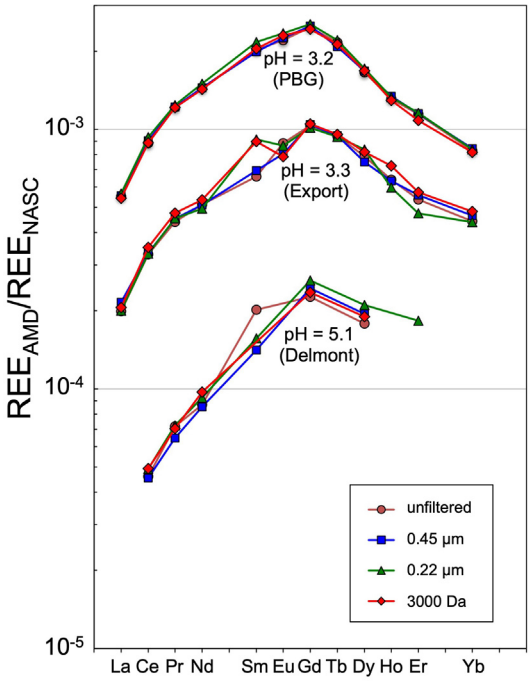

Fig. 3. Rare earth element patterns of Pittsburgh Coal mine drainage (mg/L) normalized to the North American Shale Composite (NASC, in mg/kg; Gromet et al., 1984). Each set of curves represents samples collected at the same time and filtered to different levels; particles of 3000 Da should generally be smaller than ~0.002 μm. Each curve from the Pittsburgh Botanic Garden (PBG, top) represents the average of three samples filtered to the same level. Each curve shown from the other Pittsburgh Coal discharges (Export and Delmont discharge sites) represents a single sample.

3.2. Geochemistry of whole rocks and leachates from flow path lithologies

At the Pittsburgh Botanic Garden site, rocks exposed at the strip mine are likely candidates for the lithologic units interacting with Pittsburgh Coal mine waters at depth. The extent to which individual rock types in the overburden react with mine waters depends on the distribution of lithologies, fracture patterns, and variations in water flow path and chemistry. The dominant constituents of the non-coal overburden in the area, primarily composed of quartz and aluminosilicate minerals, are Si, Al, and Fe (Table S1). The chemistry of PBG AMD is dominated by Ca, followed by Mg, Al, Si, and Na (Table S5), and reflects the relative mobility of different elements within the interacting rock units. Because of this, leachates of the whole rocks can provide more useful insight into potential contributors to AMD chemistry than can whole-rock chemistry.

The ammonium acetate (pH 8) leaches extract easily exchangeable cations that would be expected to be removed as the first slug of water moves through the system, while the sulfuric acid (0.05 M) leaches better approximate the long-term alteration/dissolution of lithologies along the AMD flow path. In general, H_2SO_4 extracted a higher load of major and trace elements (including REEs) than were extracted by ammonium acetate (Tables 1–3), with the exception of some alkali and alkaline earth metals. Notably, Ba was significantly enriched in the exchangeable fraction (Table 2), as observed in other shale leaching studies (Stewart et al., 2015; Phan et al., 2015). In general, there was little correlation between elements extracted with ammonium acetate and those extracted with H_2SO_4, with the exception of the alkaline earth elements Ca, Sr and Ba, which showed a general positive correlation.

High-valence, rock-associated cations (Si^{4+}, Al^{3+}, Fe^{3+}, Ti^{4+}) were more strongly associated with the H_2SO_4 leachate (Table 1), suggesting some involvement of silicate mineral dissolution. Based on Al and K concentrations in the leachates compared to whole-rock Al_2O_3 and K_2O contents (Table S1), the greatest amount of silicate mineral dissolution was ~0.8% (PA-PPG-SS1 sandstone), with most samples in the range of 0.1–0.6%. Other major elements in the leachate could reflect dissolution of carbonate, phosphate, and sulfide minerals. No leachate of a single lithology matched well with the PBG AMD chemistry (Table S5), indicating that the water interacted with a mixture of rock types, and could also have been affected by secondary mineral precipitation or sorption.

3.3. REE geochemistry of whole rocks and leachates

NASC-normalized whole-rock REE patterns from most silicate rock units (shale, sandstone, claystone) from the strip mine are relatively flat, with a slight light rare earth element (LREE) enrichment/heavy rare earth element (HREE) depletion, and concentrations near or above NASC (Fig. 4; Table S3). These patterns are broadly consistent with other shales and sandstones from the Appalachian Basin (Bock et al., 1994, 1998; Schatzel and

Table 1
Major elements in leachates of the Pittsburgh Botanic Garden stratigraphic section. Reported as μg of element extracted per gram of rock leached. Data determined by ICP-OES[a] at Activation Laboratories, Canada.

Sample Leach	Description	Si	Al	Fe	Mg	Mn	Ca	Na	K	Ti	P
Ammonium Acetate (NH_4Ac)											
PA-PBG-SS1	Sandstone	5.90	<1.5	<0.15	22.1	11.8	1520	5.90	42.8	<0.15	0.295
PA-PBG-15	Shale	4.55	1.52	<0.15	256	9.41	809	36.4	349	<0.15	0.304
PA-PBG-13	Shale above coal	13.9	<1.3	0.13	313	13.4	1104	22.8	232	<0.13	0.380
PA-PBG-9	Clay Parting	1.48	8.88	<0.15	62.2	1.63	54.8	<1.5	8.88	<0.15	0.444
PA-PBG-4	Coal	6.76	<1.3	4.19	16.2	<0.13	56.8	17.6	16.2	<0.13	0.541
PA-PBG-3	Clay Parting	<1.4	1.38	0.138	68.9	1.38	103	15.2	132	<0.14	<0.28
PA-PBG-1	Main Coal Seam	<1.2	<1.2	<0.12	2.51	0.125	22.6	10.0	<1.2	<0.12	0.376
PA-PBG-UC	Underclay	6.62	<1.3	0.662	379	8.74	2150	30.5	395	<0.13	5.96
Sulfuric Acid (H_2SO_4)											
PA-PBG-SS1	Sandstone	32.1	348	2770	479	109	3610	9.88	54.4	2.72	232
PA-PBG-15	Shale	374	536	13,800	594	465	1020	15.2	106	1.77	161
PA-PBG-13	Shale above coal	70.0	299	4310	112	159	709	10.6	48.8	0.637	183
PA-PBG-9	Clay Parting	83.9	800	783	19.8	3.70	7.41	<2.5	17.3	0.494	83.9
PA-PBG-4	Coal	40.6	94.7	643	6.76	0.451	15.8	2.25	9.02	0.676	18.0
PA-PBG-3	Clay Parting	156	586	419	9.16	1.83	6.87	4.58	48.1	0.458	5.49
PA-PBG-1	Main Coal Seam	<2.1	6.28	120	2.09	<0.21	8.37	<2.1	<2.1	<0.21	1.05
PA-PBG-UC	Underclay	193	667	729	102	16.2	18,100	129	195	0.886	5920

[a] Estimated uncertainty based on ActLabs QC is ≤10% of the measured value.

Stewart, 2003; Lev and Filer, 2004; Phan et al., 2018a; 2019). The mineable coal seam, which has a relatively low ash content (2.6%, representing the residual minerals after combustion; Table S1), has an order of magnitude lower REE levels than the associated silicate units. Mass balance calculations from this and other studies (Schatzel and Stewart, 2003) suggest that most of the REE are held in mineral structures rather than on or in coal particles. This is also supported by the relatively high REE content of coal with high ash content (PA-PBG-4, 49.7% ash; Table S1). The coal-associated pyrite REE concentrations are approximately two orders of magnitude lower than the silicate units and exhibit a slight HREE depletion (Fig. 4). This is similar to shale-associated pyrite from elsewhere in the Appalachian Basin (Bock et al., 1998).

Whole-rock REE patterns of the coal and overlying strata do not match those of the associated AMD, suggesting that the REE pattern of the AMD must be controlled either by selective leaching of minerals, coal, and/or rock-associated organic matter, or by sorption-desorption reactions along the flow path. The ammonium acetate leach generally yielded negligible amounts of REEs (below detection for all but sandstone PA-PBG-SS1 and clay parting PA-PBG-3; Table 3). In all cases <1% of whole-rock REEs were released into NH_4Ac leachates. In contrast, the sulfuric acid leachates of coal and overburden units contain from 0.6% to 6.9% of the total REEs, and the underclay leachate contains 34% of the total REEs in the whole rock. The REE patterns of the H_2SO_4 leachates (as well as the one full NH_4Ac leachate pattern above detection) show the characteristic MREE enrichment shared by AMD from the same site (Fig. 5). A possible exception is the H_2SO_4 leachate of the main coal seam, which appears to have a relatively flat LREE pattern but is below detection for the rest of the REEs. Given the extremely low REEs released, it is unlikely that the coal seam contributes significantly to the overall AMD REE budget.

3.4. Sr and Nd isotopes

Previous workers reported a range in $^{87}Sr/^{86}Sr$ of Pittsburgh Coal AMD from 0.71167 to 0.71264 (Capo et al., 2001; Chapman et al., 2012). The PBG AMD samples collected in 2016, along with isotope data from AMD samples collected from 1999 to 2002, fall within the reported range. Selected whole-rock samples yield significantly higher values (Table 4), consistent with silicate fractions of samples from other Appalachian shale units (Phan et al., 2018a). In contrast, most H_2SO_4 leachates yield $^{87}Sr/^{86}Sr$ ratios much lower than the whole rocks, falling relatively close to the AMD range (Fig. 6), with the exception of two samples from the clay partings.

The whole-rock $\varepsilon_{Nd}(0)$ values measured in this study (–12.0 to –11.2) are consistent with previous Nd isotope work on Appalachian Basin sedimentary rocks (Bock et al., 1994; 1998; Gleason et al., 1995; Patchett et al., 1999; Lev and Filer, 2004; Schatzel and Stewart, 2012; Phan et al., 2018a). When corrected back to the time of deposition at ~310 Ma (Table 4), $\varepsilon_{Nd}(T)$ values fall within the range expected for the isotopic evolution of the Appalachian orogen (Patchett et al., 1999).

Our results show that AMD discharges throughout the Pittsburgh Coal basin yield consistent $\varepsilon_{Nd}(0)$ values of –9.1 to –8.0 (±0.3), significantly higher than associated strata whole-rock values (Table 4). Here we also report isotope data from AMD samples collected in 1999 and 2002 from sites draining the Pittsburgh, Freeport, and Clarion Coal beds; REE concentrations from these samples were reported previously (Stewart et al., 2017). Discharges from the underlying Freeport and Clarion Coal units have $\varepsilon_{Nd}(0)$ values within the range of those of Pittsburgh Coal AMD, just as whole-rock samples from strata associated with the underlying Kittanning Coal (Schatzel and Stewart, 2012) have $\varepsilon_{Nd}(0)$ values consistent with the whole-rock data from this study.

Table 2
Trace elements in leachates of the Pittsburgh Botanic Garden stratigraphic section. Reported as μg of element extracted per gram of rock leached. Data determined by ICP-OES[a] at Activation Laboratories, Canada.

Sample Leach	Description	As	Ba	Be	Cd	Ce	Co	Cr	Cu	Li	Mo	Ni	Pb	S	Sr	Te	U	V	W	Zn
Ammonium Acetate (NH_4Ac)																				
PA-PBG-SS1	Sandstone	<0.44	1.33	<0.029	<0.029	<0.44	0.428	<0.29	0.0590	<0.74	<0.074	0.0885	<0.15	14.8	3.69	<0.15	<0.74	<0.15	0.443	0.974
PA-PBG-15	Shale	<0.45	19.3	<0.030	<0.030	<0.45	0.152	<0.30	3.20	<0.76	<0.076	0.865	<0.15	45.5	3.49	<0.15	<0.79	<0.15	<0.16	3.96
PA-PBG-13	Shale above coal	<0.38	23.7	<0.025	0.025	<0.38	0.583	<0.25	8.23	<0.63	0.0887	1.18	0.380	101	4.18	0.253	<0.63	<0.13	<0.14	4.59
PA-PBG-9	Clay Parting	<0.44	1.48	<0.030	0.133	<0.44	0.888	<0.30	11.1	<0.74	0.104	3.69	<0.15	518	0.148	0.296	<0.74	<0.15	<0.15	3.83
PA-PBG-4	Coal	<0.40	1.62	<0.027	<0.027	<0.40	0.325	<0.27	0.419	<0.68	0.0947	0.933	<0.13	352	2.03	<0.13	<0.68	<0.13	<0.13	2.12
PA-PBG-3	Clay Parting	<0.41	8.96	<0.027	0.0413	<0.41	1.50	<0.27	2.80	<0.69	0.0965	1.85	0.276	262	1.10	<0.14	<0.69	<0.14	0.276	7.08
PA-PBG-1	Main Coal Seam	<0.37	0.626	<0.025	<0.025	<0.37	0.0877	<0.25	0.213	<0.63	<0.063	0.138	<0.12	113	1.00	<0.12	<0.63	<0.12	<0.12	3.35
PA-PBG-UC	Underclay	<0.40	23.8	<0.026	0.0397	<0.40	3.83	<0.26	10.3	<0.66	0.132	12.1	<0.13	1139	29.1	<0.13	<0.66	<0.13	0.132	7.66
Sulfuric Acid (H_2SO_4)																				
PA-PBG-SS1	Sandstone	1.24	1.73	0.049	0.247	2.72	6.30	0.741	0.247	<1.2	<0.12	1.61	4.20	–	9.39	0.494	<1.2	0.988	2.22	4.79
PA-PBG-15	Shale	<0.76	3.54	0.303	1.09	2.28	3.44	1.26	2.83	<1.3	<0.13	3.03	3.29	–	4.05	1.77	1.26	4.80	<0.25	12.0
PA-PBG-13	Shale above coal	1.06	4.24	0.446	0.403	2.76	9.12	0.637	18.5	<1.1	<0.11	7.64	8.28	–	4.67	0.637	<1.1	2.55	0.212	27.8
PA-PBG-9	Clay Parting	6.17	2.22	0.198	0.247	<0.74	20.4	1.73	11.7	2.22	<0.12	3.53	0.988	–	0.247	0.494	<1.2	1.23	<0.25	15.1
PA-PBG-4	Coal	2.93	0.902	<0.045	0.0676	1.13	2.73	<0.45	1.87	<1.1	<0.11	2.14	1.80	–	0.676	<0.22	<1.1	0.451	<0.22	7.44
PA-PBG-3	Clay Parting	3.89	2.75	0.206	0.137	<0.69	17.5	0.458	5.72	1.60	<0.11	4.26	5.27	–	0.458	<0.23	<1.1	0.687	0.458	43.3
PA-PBG-1	Main Coal Seam	<0.63	<0.42	<0.042	<0.042	<0.63	0.146	<0.42	0.523	<1.0	<0.10	0.167	<0.21	–	<0.21	<0.21	<1.0	<0.21	<0.21	1.28
PA-PBG-UC	Underclay	4.87	5.76	0.487	0.133	36.1	9.13	0.665	10.3	<1.1	0.222	6.96	2.44	–	187	0.443	<1.1	0.443	<0.22	25.3

[a] Estimated uncertainty based on ActLabs QC is ≤ 10% of the measured value.

Table 3
Rare earth elements in leachates of the Pittsburgh Botanic Garden stratigraphic section. Reported as ng of element extracted per gram of rock leached. Data determined by ICP-MS[a] at the University of Pittsburgh, except where noted.

Sample	Description	La	Ce	Pr	Nd	Sm	Eu	Gd	Tb	Dy	Ho	Er	Tm	Yb	Lu	Y[b]
Ammonium Acetate (NH_4Ac)																
PA-PBG-SS1	Sandstone	72.6	176	28.4	143	64.9	21.7	87.1	14.0	74.0	15.2	39.2	<4.8	28.5	4.06	148
PA-PBG-15	Shale	<3.5	<6.2	<1.4	<1.8	<6.2	<2.1	<3.1	<0.78	<2.6	<0.80	<2.1	<0.22	<1.3	<0.27	<170
PA-PBG-13	Shale above coal	<4.6	<7.5	<0.78	<7.0	<0.45	<1.4	6.01	<0.74	<5.0	<0.73	<2.7	<0.14	<1.3	<0.055	<150
PA-PBG-9	Clay Parting	<3.6	<6.6	<0.97	<2.6	<4.4	<2.9	6.17	<0.71	<4.4	<0.38	<0.74	<0.076	<0.030	<0.035	<150
PA-PBG-4	Coal	<3.5	9.75	<1.0	<5.4	<1.3	<0.51	<1.9	<0.061	<0.83	<0.21	<0.52	<0.031	<0.37	<0.043	<230
PA-PBG-3	Clay Parting	42.2	104	17.9	107	26.0	<6.8	37.4	<4.4	<16	<3.2	<6.3	<0.54	<3.2	<0.22	<140
PA-PBG-1	Main Coal Seam	<0.74	<2.0	<0.20	<0.81	<0.50	<0.055	<0.16	<0.073	<0.16	<0.058	<0.084	<0.16	<0.059	<0.072	<120
PA-PBG-UC	Underclay	<0.75	<2.1	<0.47	<1.5	<0.22	<0.15	<0.17	<0.080	<0.60	<0.11	<0.80	<0.017	<0.25	<0.079	<130
Sulfuric Acid (H_2SO_4)																
PA-PBG-SS1	Sandstone	1030	3450	553	2860	989	261	1200	175	957	174	442	63.3	374	51.2	3460
PA-PBG-15	Shale	791	3156	534	3312	1462	376	2020	276	1175	187	415	50.4	257	38.0	4050
PA-PBG-13	Shale above coal	896	3542	572	3288	1370	388	2048	283	1409	224	512	62.7	352	46.4	4670
PA-PBG-9	Clay Parting	98.5	403	77.1	481	182	47.1	213	25.8	157	26.3	76.1	<9.9	52.2	7.68	494
PA-PBG-4	Coal	405	1370	177	758	172	35.8	152	18.8	82.3	12.2	25.5	<2.8	17.9	1.85	<220
PA-PBG-3	Clay Parting	164	695	117	570	168	45.7	269	44.9	258	46.8	121	<15.0	102	14.2	687
PA-PBG-1	Main Coal Seam	19.6	44.1	<5.4	18.3	<5.5	<1.2	<5.0	<0.43	<2.4	<0.31	<0.72	<0.07	<0.60	<0.22	<210
PA-PBG-UC	Underclay	15,100	48,100	6860	29,600	7090	1630	7840	1160	6670	1210	2790	311	1490	172	28,100

[a] Estimated uncertainties are ≤10% of the measured value.
[b] Yttrium determined by ICP-OES (Activation Laboratories, Canada).

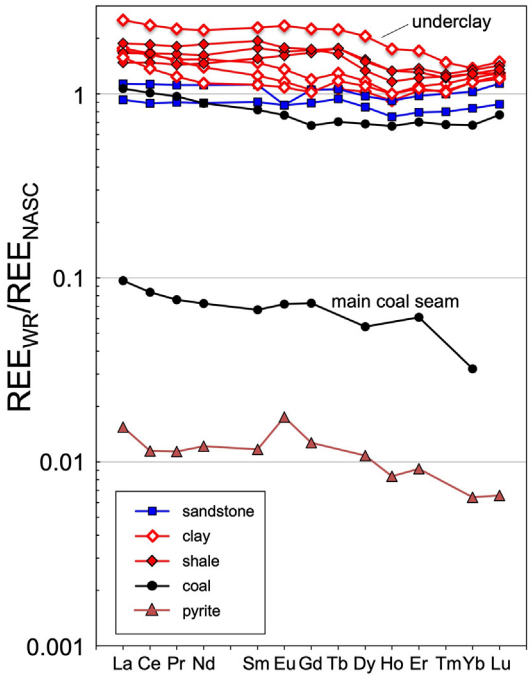

Fig. 4. NASC-normalized rare earth element patterns of rock units from the Pittsburgh Botanic Garden (PBG) strip mine site, representing likely lithologies that interact with Pittsburgh Coal mine drainage. The pyrite was separated from a coal sample collected at the field site.

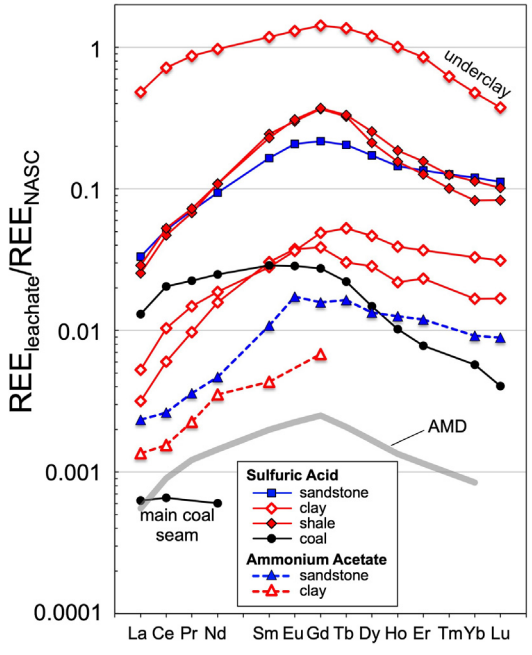

Fig. 5. NASC-normalized rare earth element patterns of NH_4Ac (dashed lines) and H_2SO_4 (solid lines) leachates of different lithologies from the PBG site. Leachate concentrations (prior to NASC normalization) are μg of rare earth element extracted per g of rock leached. The REE pattern of AMD, shown to allow comparison to the leachates, consists of the average of REE concentrations (mg/L prior to NASC normalization) from three samples from the PBG site.

While ammonium acetate and H_2SO_4 leachates yield a relatively wide range of $\varepsilon_{Nd}(0)$ values, all but the underclay H_2SO_4 leachate (PA-PBG-UC) fall significantly above whole-rock values, and generally span the AMD values. The underclay H_2SO_4 leachate, in addition to having very high REE concentrations, also has $\varepsilon_{Nd}(0)$ values similar to those of the whole rocks.

4. DISCUSSION

4.1. Contributors to AMD chemistry

Acid mine drainage interacts with a wide variety of lithologies along its flow path. The water table in below-drainage deep mines can be well above the mined coal seam, allowing mine water to interact with stratigraphically shallower units. Likewise, the water table in above-drainage mines, such as the abandoned deep-mine at the Pittsburgh Botanic Garden, can also lie above the mined coal seam (Hobba, 1993). Moreover, overburden material that has collapsed into mine voids can interact with AMD and increase permeability in stratigraphically shallower units (Singh and Kendorski, 1981; Hobba, 1993; Kendorski, 2006). As Pittsburgh Coal mines exhibit both above and below drainage hydrology (Winters and Capo, 2004), potential contributors to AMD geochemistry include unmined coal, clay units and tonsteins, and sedimentary lithologies such as shales, sandstones, and limestones (where present). As noted previously, major and trace element data cannot uniquely identify the major contributors to the dissolved load of AMD, given the wide range of extractable compositions and potential precipitation and sorption reactions along the flow path. Based on the amounts of metals released by H_2SO_4 leaching (Table 1), unmined coal does not appear to be a major contributor, and mass balance calculations indicate that pyrite does not appear to be capable of contributing significant major elements other than Fe (Table S1), even though its dissolution is the major source of acidity and sulfur. Thus, the silicate units (shale, sandstone, clay partings, and underclay) are all potential sources of cations to the AMD.

The $^{87}Sr/^{86}Sr$ ratios of the H_2SO_4 leachates span the range of values observed in Pittsburgh Coal AMD (Fig. 6), indicating that released Sr from these different lithologies contributes to the overall signature. While leachates of the clay partings fall well outside of the range of AMD values, the very low concentrations of extractable Sr suggest that their contribution to the Sr budget is minimal. The amount of H_2SO_4-extractable Sr of the underclay is more than an order of magnitude greater than that of the shales or sandstone. It would be expected that the isotopic signature of the underclay would likely dominate the AMD if the mine waters had interacted with the underclay. However, Pittsburgh Coal AMD discharges measured to date (Chapman et al., 2012; Sharma et al., 2013; Table 4) have a significantly higher $^{87}Sr/^{86}Sr$ than the underclay leachate (Fig. 6), which suggests minimal interaction of mine waters with underclay. This is consistent with physical models of room-and-pillar mine collapse in which the overburden is fractured and permeable, while the mine floor (underclay)

Table 4
Nd and Sr isotope data for whole-rock and leachate samples of the Pittsburgh Botanic Garden stratigraphic section, and for acidic coal mine drainage from western Pennsylvania.

Sample	Description	$^{87}Sr/^{86}Sr$[a,b]	$^{147}Sm/^{144}Nd$[c]	$\varepsilon_{Nd}(0)$[b,d]	$\varepsilon_{Nd}(310\ Ma)$[d,e]
Solid Samples					
PA-PBG-SS1 Whole Rock	Sandstone	0.72003 ± 0.00003	0.1192	−11.18 ± 0.12	−8.11 ± 0.43
PA-PBG-3 Whole Rock	Clay Parting	0.72333 ± 0.00002	0.1164	−12.02 ± 0.16	−8.85 ± 0.48
PA-PBG-UC Whole Rock	Underclay	0.71457 ± 0.00002	0.1231	−11.53 ± 0.12	−8.62 ± 0.42
PA-PBG-PY1	Pyrite separate	0.71128 ± 0.00003			
Ammonium Acetate (NH_4Ac) Leachate					
PA-PBG-SS1	Sandstone	0.71173 ± 0.00002	0.2748	−5.77 ± 0.14	−8.88 ± 0.45
PA-PBG-3	Clay Parting	0.72010 ± 0.00002	0.1462	−8.08 ± 0.14	−6.09 ± 0.34
Sulfuric Acid Leachate (0.05M)					
PA-PBG-SS1	Sandstone	0.71160 ± 0.00002	0.2089	−6.10 ± 0.20	−6.59 ± 0.25
PA-PBG-15	Shale	0.71311 ± 0.00002	0.2670	−7.13 ± 0.12	−9.92 ± 0.40
PA-PBG-13	Shale above coal	0.71186 ± 0.00002	0.2521	−6.23 ± 0.12	−8.43 ± 0.34
PA-PBG-9	Clay Parting	0.71942 ± 0.00003	0.2288	−6.80 ± 0.11	−8.08 ± 0.24
PA-PBG-4	Coal	0.71303 ± 0.00002	0.1376	−9.28 ± 0.12	−6.94 ± 0.36
PA-PBG-3	Clay Parting	0.72209 ± 0.00003	0.1778	−7.87 ± 0.14	−7.12 ± 0.21
PA-PBG-1	Main Coal Seam	0.71084 ± 0.00003			
PA-PBG-UC	Underclay	0.71104 ± 0.00002	0.1446	−11.02 ± 0.15	−8.97 ± 0.36
Acid Mine Drainage					
Hope Hollow 2/28/2002	Pittsburgh Coal		0.2057	−8.05 ± 0.20	−8.42 ± 0.24
Whiskey Run 2/28/2002	Pittsburgh Coal		0.1803	−8.67 ± 0.32	−8.02 ± 0.38
PBG 2/28/2002	Pittsburgh Coal		0.1869	−8.82 ± 0.33	−8.44 ± 0.37
PBG 3/8/2016	Pittsburgh Coal	0.71184 ± 0.00002	0.1756	−9.13 ± 0.57	−8.30 ± 0.65
Delmont 3/3/1999	Pittsburgh Coal	0.71252 ± 0.00005	0.2044	−8.19 ± 0.25	−8.50 ± 0.28
Export 3/3/1999	Pittsburgh Coal	0.71242 ± 0.00001	0.1899	−8.65 ± 0.14	−8.39 ± 0.16
McLaughlin 2/28/2002	Pittsburgh Coal			−7.96 ± 0.23	
Waterman 6/17/1999	Freeport Coal	0.71417 ± 0.00001	0.2253	−8.32 ± 0.29	−9.46 ± 0.40
Filson 7/9/1999	Clarion Coal		0.1478	−9.29 ± 0.27	−7.35 ± 0.46

[a] AMD $^{87}Sr/^{86}Sr$ data from Delmont, Export, and Waterman discharges were analyzed by TIMS and reported by Chapman et al. (2012); all other data were analyzed by MC-ICP-MS. All values are normalized to NIST SRM 987 = 0.710240.
[b] Quoted isotope uncertainties shown are 2 × the standard error of the mean.
[c] Uncertainty in the $^{147}Sm/^{144}Nd$ ratio is ≤ 10% based on analytical uncertainties of Sm and Nd measurements.
[d] $\varepsilon_{Nd}(T) = [^{143}Nd/^{144}Nd(T)_{sample}/^{143}Nd/^{144}Nd(T)_{CHUR} - 1]10^4$, where $^{143}Nd/^{144}Nd(0)_{CHUR} = 0.511847$.
[e] Quoted uncertainties in $\varepsilon_{Nd}(310\ Ma)$ incorporate uncertainty in the measured $^{147}Sm/^{144}Nd$ ratio.

remains relatively impermeable (Singh and Kendorski, 1981; Kendorski, 2006). Based on the results presented here, the shale and sandstone units appear to be the primary contributors of Sr (and therefore Ca) to Pittsburgh Coal AMD.

The observation that the H_2SO_4 leachates of silicates in the stratigraphic section have lower $^{87}Sr/^{86}Sr$ ratios than the corresponding whole rocks (where measured) obviates the need to invoke AMD dissolution of discrete marine limestone units to balance out the high ratios of the shale units (Capo et al., 2001). Instead, it is likely that these rocks contain one or more relatively soluble phases that have maintained a lower Rb/Sr ratio than the whole rock since the time of deposition. The most likely candidates are carbonate minerals (calcite or dolomite) that crystallized as a fine-grained cement during diagenesis. Previous shale leaching studies show that carbonate cement can yield $^{87}Sr/^{86}Sr$ ratios well below those of the shale whole rock, approaching paleo-seawater values (Stewart et al., 2015). Siderite nodules (syn-depositional or diagenetic) are another potential source of low-$^{87}Sr/^{86}Sr$ strontium in AMD (Chapman et al., 2013), although none were observed in the samples leached in this study.

4.2. Controls on rare earth element patterns in acid mine drainage

4.2.1. Constraints from leachate REE extraction

Leaching experiments on lithologies associated with the Pittsburgh Coal seam show that most leachates yield MREE-enriched patterns characteristic of mine drainage (Fig. 5), and distinct from any of the whole-rock REE patterns (Fig. 4). Comparison of ammonium acetate and H_2SO_4 leachates indicates that surface-bound REEs, including those on coal particles, do not contribute significantly to AMD REE budgets. In contrast, simulated AMD (H_2SO_4) extracts up to 35% of the rock's total REEs (underclay PA-PBG-UC), with most samples yielding 1–7% of their total REEs. The REE abundances and patterns could reflect a variety of processes, including dissolution of soluble minerals, colloidal fractionation, and sorption-desorption processes within the mine pool.

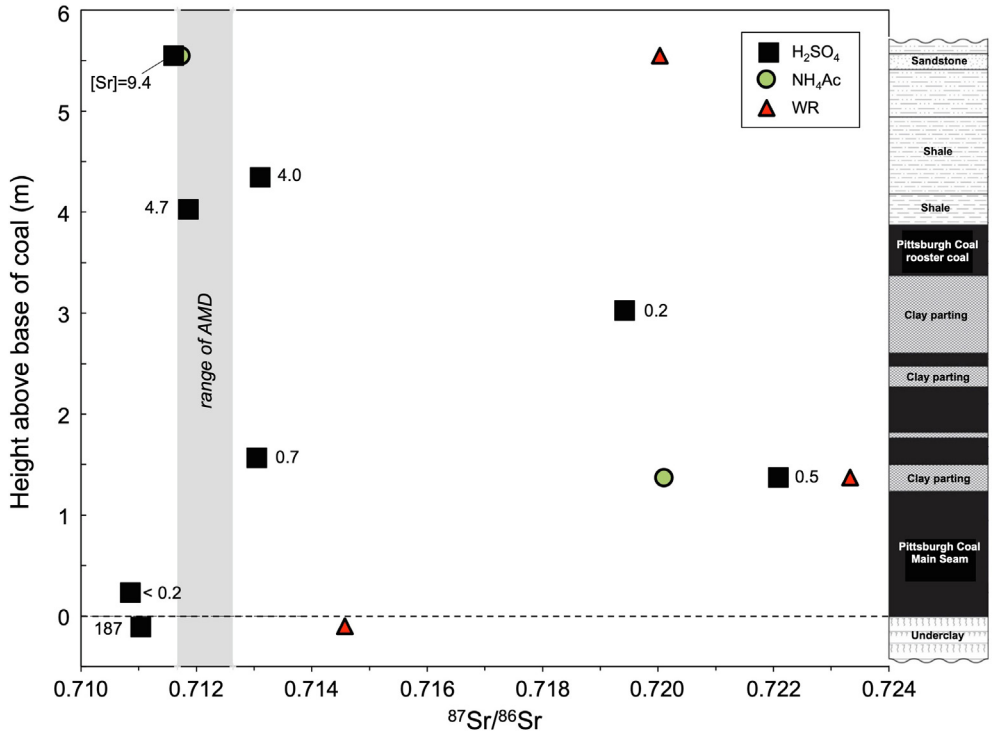

Fig. 6. Sr isotope variations as a function of stratigraphic height from sulfuric acid (H_2SO_4) and ammonium acetate (NH_4Ac) leachates and whole-rock (WR) samples associated with the Pittsburgh Coal. The gray line represents the range of Pittsburgh Coal AMD values reported by Chapman et al. (2012) and this study. The numbers labeling individual H_2SO_4 leachate data points are the concentration of Sr extracted (μg of Sr per g of sample leached).

Comparisons of leachate REE concentrations (reported as μg of leachable REE per g of rock) with AMD REE concentrations suggest water/rock ratios of 10^1–10^2 to generate AMD with similar REE content. The leachate patterns differ significantly from the associated whole-rock REE patterns, and suggest that one or more phases with distinct REE patterns are selectively leached by the H_2SO_4 to produce the characteristic MREE enrichment. However, even with the relatively short duration of the experiments, we could not rule out the possibility of sorption-desorption reactions controlling the characteristic REE patterns.

4.2.2. Selective dissolution vs. process-driven REE fractionation

Observed REE patterns (including MREE enrichment) in ground and surface water can be attributed to selective dissolution of soluble minerals, or to process-driven fractionation mechanisms such as mineral surface reactions controlled by REE speciation and aqueous complexation, incongruent dissolution of minerals such as pyrite, and/or solid-liquid exchange reactions and precipitation of secondary minerals. In addition, colloids have been suggested to play an important role in REE patterns and solubility in ground and surface waters (Hoyle et al., 1984; Elderfield et al., 1990; Sholkovitz, 1992; Zhang et al., 1998; Dupré et al., 1999; Ingri et al., 2000; Dia et al., 2000; Andersson et al., 2001), as well as in waters affected by acidic runoff (Åström, 2001; Verplanck et al., 2004; Sun et al., 2012). However, the consistent REE patterns and concentrations between unfiltered AMD and filtrates ranging to ~0.002 μm (Fig. 3) indicate that colloids are not a significant carrier of REE in these samples and are not responsible for the observed MREE-enriched patterns.

To discriminate between selective dissolution and process-driven fractionation in Appalachian coal AMD, we applied Nd isotopes to AMD discharges, solid samples and leachates. Neodymium isotopes can effectively differentiate recent REE fractionation (*i.e.*, since the onset of AMD) from extraction of minerals with REE patterns inherited at the time of deposition in the late Carboniferous. Minerals with a MREE-enriched pattern inherited at the time of deposition will have a relatively high Sm/Nd ratio, and thus generate higher ε_{Nd} values in the present day ($\varepsilon_{Nd}(0)$) due to decay of ^{147}Sm over the ~310 m.y. since deposition. In contrast, minerals that evolved from the time of deposition with shale-like REE patterns (relatively flat NASC-normalized) will have lower Sm/Nd ratios, and thus lower $\varepsilon_{Nd}(0)$ values even if their REE are fractionated during AMD generation.

Despite the clear distinction in measured $\varepsilon_{Nd}(0)$ values between AMD and the whole rock, when the Nd isotope ratio is calculated back to the time of deposition of the Pittsburgh Coal (~310 Ma), using measured $^{147}Sm/^{144}Nd$ ratios to account for ^{147}Sm decay, both sets of data converge to a narrow range of $\varepsilon_{Nd}(310\ Ma)$ values (–8.8 to –8.0; Table 4). This is illustrated in Fig. 7a: The whole rock, with a low Sm/Nd ratio at 310 Ma, evolves toward lower $\varepsilon_{Nd}(T)$ values to the present day, whereas the

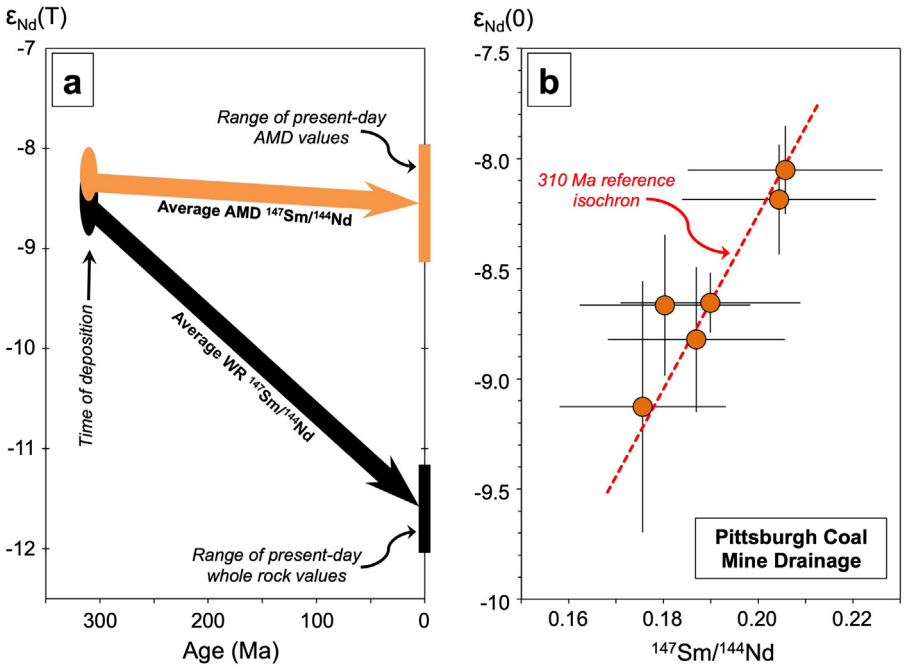

Fig. 7. a. Model showing Nd isotope evolution (black arrow) of whole-rock samples from the time of deposition to the present day (range indicated with black vertical bar). The orange arrow indicates the Nd isotope evolution of a hypothetical phase that is sequentially leached to produce present-day AMD; the slope of the evolutionary paths is determined by the average of the measured Sm/Nd ratios of the whole rocks and the Pittsburgh Coal AMD samples from this study. b. Pseudo-isochron diagram showing individual AMD samples from different discharges within the Pittsburgh Coal, with a reference 310 Ma isochron (representing the time of deposition).

components (minerals or organic matter) within the rock that are selectively dissolved by AMD have a higher Sm/Nd than the whole rock, and thus have a higher $\varepsilon_{Nd}(T)$ today. This suggests that AMD selectively leaches one or more minerals associated with deposition of the coal and the adjacent strata, and that these phases have higher Sm/Nd ratios (with associated MREE-enriched patterns) that are distinct from the bulk silicate rock in which they reside. This process has been suggested to operate during weathering of crustal rocks and sediments, leading to divergence between marine and continental Nd isotope records (Hindshaw et al., 2018).

If the MREE-enriched patterns were generated at the time of AMD formation through the process-driven mechanisms listed above, Sm/Nd ratios of AMD should be decoupled from the $\varepsilon_{Nd}(0)$ values of the source minerals. However, our data show that individual discharges from different parts of the Pittsburgh Coal basin define a trend on an isochron diagram consistent with the ~310 Ma age of the Pittsburgh Coal (Fig. 7b). This indicates that they faithfully reproduce the long-term Sm/Nd ratio of their source. Fractionation of Sm/Nd during or after leaching from minerals in the mine pool would lead to diverging $\varepsilon_{Nd}(T)$ values for AMD, which is not observed. Control of the REE patterns in these AMD samples by incongruent dissolution (Grawunder et al., 2014) is therefore ruled out by the Nd isotope data. These data also show that post-dissolution processes, such as selective fractionation by colloids and sorption-desorption reactions, are not responsible for the REE patterns within the range of pH values for this study (≤5.1). This is consistent with the observations of Verplanck et al. (2004) that REE are not adsorbed by or co-precipitated with Fe oxyhydroxides at pH < 5.1. The REE in circumneutral mine drainage (as opposed to AMD) could be more strongly affected by adsorption/co-precipitation processes, although Stewart et al. (2017) showed that several Appalachian coal mine drainages with pH > 5.1 displayed similar MREE-enriched patterns as AMD.

Exchangeable cations and simulated mine drainage (H_2SO_4) leachates of units associated with the Pittsburgh Coal yield a relatively wide range of $\varepsilon_{Nd}(0)$ values that are nonetheless consistent with Pittsburgh Coal AMD (Table 4). The simulated AMD leachates give an $\varepsilon_{Nd}(0)$ range of –11.0 to –6.1, with an average of –7.8 (compared to an average value of –8.5 for Pittsburgh Coal AMD). This indicates that the simulated AMD leachates are targeting similar mineral phases as actual AMD in the mine pool. The H_2SO_4 leachate of the underclay immediately below the main seam of the Pittsburgh coal (PA–PBG–UC) is somewhat anomalous in terms of the amount of REEs leached (~34% of the total in the rock), its less pronounced LREE depletion (Fig. 5), and its Nd isotopic composition. Pedogenic processes prior to and during deposition of the coal mire may have redistributed REEs from the parent sediment into authigenic phases that are relatively soluble in H_2SO_4. However, based on the $\varepsilon_{Nd}(0)$ value of the leachate ($\varepsilon_{Nd}(0) = -11.0$), this unit does not appear to contribute significantly to AMD ($\varepsilon_{Nd}(0) = -9.1$ to –8.0), which is consistent with our findings from the $^{87}Sr/^{86}Sr$ ratios (Section 4.1).

When the $\varepsilon_{Nd}(T)$ values of the simulated mine drainage leachates are calculated back to the time of deposition (T = 310 Ma), they converge to a narrow range of –9.9 to –6.6 (average –8.0) (Table 4), indicating that the sulfuric acid is targeting phases with Sm/Nd ratios (therefore REE patterns) and $\varepsilon_{Nd}(T)$ values inherited at the time of deposition, similar to what is inferred for the AMD. When all the data are considered together (whole rocks, AMD and leachates, including the anomalous underclay PA-PBG-UC), they define a trend consistent with the 310 Ma depositional age of the Pittsburgh Coal (Fig. 8). The scatter off of the reference isochron in this diagram likely reflects the variation in sediment sources within the overlying units at the time of deposition. The relatively tight clustering of AMD data (collected from different discharges from the Pittsburgh coal seam) relative to the H_2SO_4 leachates indicates that AMD interacts with and inherits its REE from a restricted portion of the overlying stratigraphy. These data support a model in which (1) sediments with Nd isotope compositions and REE patterns consistent with other Appalachian Basin shales and sandstones were deposited and coal mires developed at ~310 Ma (Gleason et al., 1994; Bock et al., 1994; 1998; Patchett et al., 1999; Lev and Filer, 2004; Schatzel and Stewart, 2012; Phan et al., 2018a); (2) mineral or organic-rich phases enriched in MREEs formed within the Pittsburgh Coal and associated strata at or soon after the time of deposition by pedogenic and diagenetic processes, inheriting the whole-rock $\varepsilon_{Nd}(T)$ values; (3) the $\varepsilon_{Nd}(T)$ of the MREE-enriched phase and the whole rock diverged over the subsequent ~300 million years due to their different Sm/Nd ratios (Fig. 7a); and (4) the MREE-enriched phase was selectively dissolved by acidic mine waters.

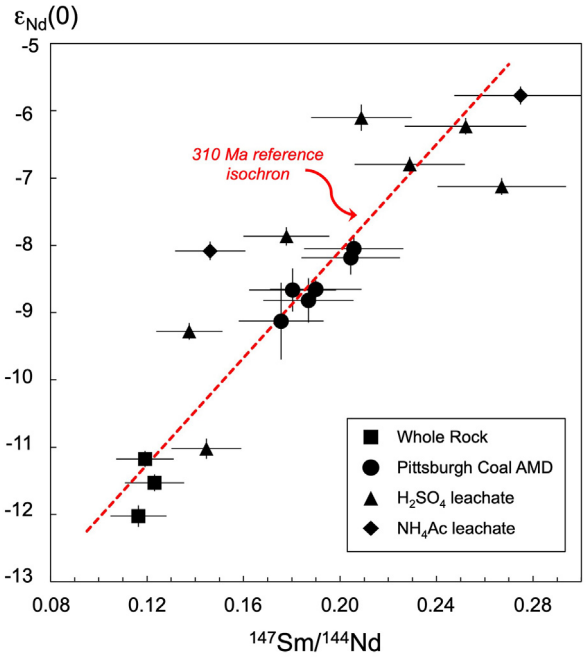

Fig. 8. Pseudo-isochron for Sm-Nd data from this study, including AMD from the Pittsburgh Coal, whole-rock samples, and leachates.

4.2.3. Source of REEs in mine waters

Our data demonstrate that the REE patterns in mine drainage result from selective leaching of one or more relatively soluble minerals in the mine rock and overburden that react with the AMD. These minerals have MREE-enriched patterns inherited near the time of coal deposition that are passed on to the AMD. Moreover, the isotope data show that little to no fractionation of the Sm/Nd ratio (and thus likely of the REE pattern as a whole) takes place once the REEs are released into solution in the mine pool prior to discharge, as this would lead to large variations in $\varepsilon_{Nd}(T)$ values calculated at 310 Ma, the time of coal deposition.

One approach to determine the likely sources of REEs to AMD is to compare REE concentrations to the major and minor element chemistry of the waters to back out the likely dissolving phases. However, sorption and precipitation reactions can mask the identity of the original REE sources. For example, low concentrations of P in coal mine drainage likely reflect rapid adsorption on Fe and Al phases within the mine pool (e.g., Hongshao and Stanforth, 2001; Ler and Stanforth, 2003; Genz et al., 2004; Cravotta, 2008a). In the relatively short duration simulated AMD leaching experiments, such reactions could be more limited, thus allowing insight into the likely REE sources. We compared Nd concentrations (as a proxy for REEs) to phosphorus (P) released during the simulated AMD experiments (Fig. 9). A linear correlation is observed between P and Nd ($R^2 = 0.99$, or 0.82 if the high P, Nd sample PA-PBG-UC is excluded). This is notable, as the mineral apatite ($Ca_5(PO_4)_3(OH,F,Cl)$) and related phosphates such as carbonate fluorapatite (CO_3 in carbonate partially replaced by PO_4 during diagenesis; Ames, 1959) are potential candidates as sources of REE in AMD. Shale-normalized phosphate REE patterns often show MREE enrichment (Kidder and Eddy-Dilek, 1994; Bouch et al., 2002; Kidder et al., 2003; Lev and Filer, 2004; Chen et al., 2015; Joosu et al., 2016; Trotter et al., 2016; Zhang et al., 2016; Mao et al., 2016; Yang et al., 2017), and phosphate minerals have been suggested as a potential source for the MREE-enriched patterns found in some acidic natural waters (Hannigan and Sholkovitz, 2001; Aubert et al., 2001; García et al., 2007).

Neodymium concentrations in apatite can range from <100 to >8000 ppm, with some of the highest concentrations reported in authigenic apatite formed during diagenesis (Bouch et al., 2002). For the rocks leached in this study, both the potential amount of apatite and the concentration of Nd in the apatite are likely to be highly variable. We calculated the amount of Nd released as a function of P concentration in the leachate for a range of Nd concentrations [Nd], assuming all the P and Nd is from apatite (dashed lines, Fig. 9). Most of the range of [Nd] in the leachates could be explained by apatite dissolution, albeit some requiring apatite with Nd concentrations up to 5000 ppm. If a significant portion of the P is resorbed by the sample, even during this relatively short experiment, then the calculated amount of apatite dissolved would be an underesti-

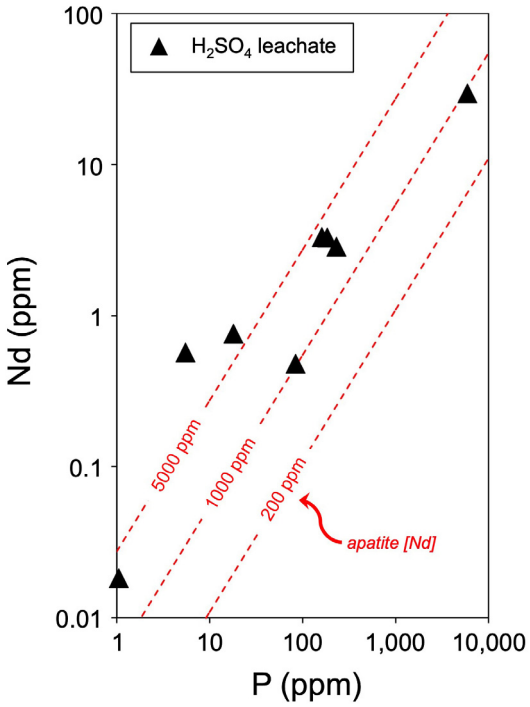

Fig. 9. Relationship between Nd and P concentrations of the simulated AMD (0.05 M H_2SO_4) leachates. The dashed lines indicate the expected relationships for release of Nd and P for different Nd concentrations in apatite.

mate, and the required Nd concentration of the apatite would proportionally decrease. We conclude that apatite and/or a related phosphate mineral could account for most of the REE signal observed in our leachates.

An additional possible source of REEs is carbonate minerals, either as limestone in the overburden or as carbonate cement in shales or sandstones. Although no carbonate minerals were directly observed in the lithologic units studied here, some Appalachian organic-rich black shales are known to contain significant carbonate cement (Stewart et al., 2015; Yang et al., 2017; Phan et al., 2018a), which can also have MREE-enriched REE patterns (Phan et al., 2018a; 2019). The Ca/P ratio of most leachates exceeds that of apatite (Ca/P mass ratio of 2.16), and this additional Ca could be contributed by carbonate dissolution. Although carbonate cement could be a primary contributor of Sr (with low $^{87}Sr/^{86}Sr$) in AMD, carbonate minerals have relatively low REE concentrations (generally much less than 150 ppm; Phan et al., 2018a; 2019), and are likely to be only a minor contributor to the total AMD REE budget.

Given that phosphate appears to be the dominant source of REEs, we can calculate the approximate resources available in a given AMD flow path or tailing pile. Total P_2O_5 in the rocks interacting with the AMD ranged from ~0.05 to 0.25 wt. % (average of 0.15%; Table S1), excluding the mined coal and the underclay. If most of the phosphate is in the form of apatite, this translates to 0.1–0.6% apatite (average 0.36%), consistent with apatite content in clastic units throughout the Appalachian Basin (Reed et al., 2005a; 2005b; Lebold and Kammer, 2006; Wang and Carr, 2013). For apatite with a Nd concentration of 1000 ppm, this would correspond to 3.6 g of easily extractable Nd per metric ton of rock leached by AMD. While this does not represent ore-grade material (which can range from <250 to 21,500 ppm Nd; Kanazawa and Kamitani, 2006; Van Gosen et al., 2017), the advantage is that the extraction is already occurring in systems that are currently producing AMD, which can then be treated at the source to concentrate REEs (Stewart et al., 2017). Our study suggests that mine drainage interacting with phosphate-rich lithologies has the potential to yield economic quantities of REEs.

5. CONCLUSIONS

We carried out a comparative geochemical and isotopic study of Appalachian coal mine drainage and AMD-simulating leachates of the rock units associated with mine drainage to determine the source of REE in mine discharges and acidic groundwaters. Our primary findings:

- Based on filtration experiments, the REEs in coal mine drainage are not bound to or fractionated by colloids, even in waters with pH as high as 5.1 (Fig. 3). Both unfiltered and filtered (to a level of ~0.002 μm) mine drainage have essentially identical REE concentrations and patterns.
- Simulated AMD (0.05 M H_2SO_4) leachates of rock units associated with coal mine drainage yield MREE-enriched patterns similar to those observed in coal mine drainage. Comparison with ammonium acetate (pH 8) leachates shows that cation exchange sites contribute negligible amounts of REEs, and that coal units themselves are not a major source of REEs. Instead, overlying shale and clay units appear to be the primary contributors of REEs to coal AMD. Concentrations of REEs released suggest water/rock mass ratios of 10^1–10^2 to produce the observed REE concentrations in coal mine drainage.
- Simulated AMD leachates of rock units yield fluids with lower $^{87}Sr/^{86}Sr$ ratios than the whole rock (where measured) and are broadly consistent with AMD from the Pittsburgh coal. An important source of Sr (and potentially Ca and Mg) could be carbonate cement in the overlying shales and clays. However, carbonate is unlikely to contain enough REEs to contribute significantly to the overall REE patterns of AMD.
- While the underclay at the floor of the abandoned coal mine has unusual chemistry and very high Sr and REE contents (including H_2SO_4-leachable REE), the $^{87}Sr/^{86}Sr$ isotope data from coal mine drainage and leachates indicates that the mine waters interact only minimally with this unit. This is consistent with physico-hydrologic models for mine overburden fracturing and AMD interaction (Singh and Kendorski, 1981; Hobba, 1993; Kendorski, 2006), and it rules out the underclay as a major source of REE in coal mine drainage.
- Neodymium isotope data show that coal mine drainage inherits its Sm/Nd ratio (and hence, likely its overall REE pattern) from selective dissolution of mineral(s) that formed at or near the time of deposition in the late

Carboniferous. These data are not consistent with models where the REE pattern is produced by incongruent dissolution of minerals such as pyrite or sorption/desorption reactions in the mine pool.

- The REE patterns and REE/P abundances are consistent with phosphate dissolution combined with sorption of P along the mine flow path. The primary source of REE in coal mine drainage, and potentially to other acidic discharges, could be phosphate minerals (e.g., apatite) inherited from the source region or formed by authigenic or diagenetic processes.

Declaration of Competing Interest

The authors declare that they have no known competing financial interests or personal relationships that could have appeared to influence the work reported in this paper.

ACKNOWLEDGEMENTS

We thank the Pittsburgh Botanic Garden for sampling access to AMD and associated rock units. We appreciate the careful and constructive manuscript reviews by J. Rickli and an anonymous reviewer, and we thank Editor-in-Chief J. Catalano for handling the manuscript. Partial support for this project was provided by the University of Pittsburgh Central Research Development Fund (RCC) and a J. Frederick and Ann Sarg Award (ILRW).

APPENDIX A. SUPPLEMENTARY MATERIAL

Supplementary data to this article can be found online at https://doi.org/10.1016/j.gca.2019.10.044.

REFERENCES

Akcil A. and Koldas S. (2006) Acid Mine Drainage (AMD): causes, treatment and case studies. *J. Clean. Prod.* **14**, 1139–1145.

Ames, Jr., L. L. (1959) The genesis of carbonate apatites. *Econ. Geol.* **54**, 829–841.

Andersson P. S., Dahlqvist R., Ingri J. and Gustafsson Ö. (2001) The isotopic composition of Nd in a boreal river: A reflection of selective weathering and colloidal transport. *Geochim. Cosmochim. Acta* **65**, 521–527.

Åström M. (2001) Abundance and fractionation patterns of rare earth elements in streams affected by acid sulphate soils. *Chem. Geol.* **175**, 249–258.

Åström M. and Corin N. (2003) Distribution of rare earth elements in anionic, cationic and particulate fractions in boreal humus-rich streams affected by acid sulphate soils. *Wat. Res.* **37**, 273–280.

Aubert D., Stille P. and Probst A. (2001) REE fractionation during granite weathering and removal by waters and suspended loads: Sr and Nd isotopic evidence. *Geochim. Cosmochim. Acta* **65**, 387–406.

Ayora C., Macias F., Torres E., Lozano A., Carrero S., Nieto J. M., Perez-Lopez R., Fernandez-Martinez A. and Castillo-Michel H. (2016) Recovery of rare earth elements and yttrium from passive-remediation systems of acid mine drainage. *Environ. Sci. Technol.* **50**, 8255–8262.

Banner J. L. (2004) Radiogenic isotopes: systematics and applications to earth surface processes and chemical stratigraphy. *Earth-Sci. Rev.* **65**, 141–194.

Bau M. and Möller P. (1993) Rare earth element systematics of the chemically precipitated component in Early Precambrian iron formations and the evolution of the terrestrial atmosphere-hydrosphere-lithosphere system. *Geochim. Cosmochim. Acta* **57**, 2239–2249.

Binnemans K., Jones P. T., Blanpain B., Van Gerven T., Yang Y., Walton A. and Buchert M. (2013) Recycling of rare earths: a critical review. *J. Clean. Prod.* **51**, 1–22.

Blowes D. W., Ptacek C. J., Jambor J. L., Weisener C. G., Paktunc D., Gould W. D. and Johnson D. B. (2014) The geochemistry of acid mine drainage. In *Environmental Geochemistry* (ed. B. Sherwood Lollar). Elsevier, pp. 131–190.

Bock B., McLennan S. M. and Hanson G. N. (1994) Rare earth element redistribution and its effects on the neodymium isotope system in the Austin Glen Member of the Normanskill Formation, New York, USA. *Geochim. Cosmochim. Acta* **58**, 5245–5253.

Bock B., McLennan S. M. and Hanson G. N. (1998) Geochemistry and provenance of the Middle Ordovician Austin Glen Member (Normanskill Formation) and the Taconian Orogeny in New England. *Sedimentology* **45**, 635–655.

Bouch J. E., Hole M. J., Trewin N. H., Chenery S. and Morton A. C. (2002) Authigenic apatite in a fluvial sandstone sequence: Evidence for rare-earth element mobility during diagenesis and a tool for diagenetic correlation. *J. Sed. Res.* **72**, 59–67.

Capo R. C., Stafford S. L., Kairies C. L., Stewart B. W. and Hedin R. S. (2001) Strontium and neodymium isotopic composition of coal mine drainage as a tracer of subsurface geochemistry. In *Proceedings of the 4th International Symposium on Applied Isotope Geochemistry, Pacific, CA*, pp. 155–157.

Capo R. C., Stewart B. W. and Chadwick O. A. (1998) Strontium isotopes as tracers of ecosystem processes: Theory and methods. *Geoderma* **82**, 197–225.

Capo R. C., Stewart B. W., Rowan E. L., Kolesar Kohl C. A., Wall A. J., Chapman E. C., Hammack R. W. and Schroeder K. T. (2014) The strontium isotopic evolution of Marcellus Formation produced waters, southwestern Pennsylvania. *Int. J. Coal Geol.* **126**, 57–63.

Chapman E. C., Capo R. C., Stewart B. W., Hedin R. S., Weaver T. J. and Edenborn H. M. (2013) Strontium isotope quantification of siderite, brine, and acid mine drainage contributions to abandoned gas well discharges in the Appalachian Plateau. *Appl. Geochem.* **31**, 109–118.

Chapman E. C., Capo R. C., Stewart B. W., Kirby C. S., Hammack R. W., Schroeder K. T. and Edenborn H. M. (2012) Geochemical and strontium isotope characterization of produced waters from Marcellus Shale natural gas extraction. *Environ. Sci. Technol.* **46**, 3545–3553.

Chen J., Algeo T. J., Zhao L., Chen Z.-Q., Cao L., Zhang L. and Li Y. (2015) Diagenetic uptake of rare earth elements by bioapatite, with an example from Lower Triassic conodonts of South China. *Earth-Sci. Rev.* **149**, 181–202.

Cole R. B. and Stewart B. W. (2009) Continental margin volcanism at sites of spreading ridge subduction: Examples from southern Alaska and western California. *Tectonophysics* **464**, 118–136.

Coppin F., Berger G., Bauer A., Castet S. and Loubet M. (2002) Sorption of lanthanides on smectite and kaolinite. *Chem. Geol.* **182**, 57–68.

Cravotta, III, C. A. (2008a) Dissolved metals and associated constituents in abandoned coal-mine discharges, Pennsylvania, USA. Part 1: Constituent quantities and correlations. *Appl. Geochem.* **23**, 166–202.

Cravotta, III, C. A. (2008b) Dissolved metals and associated constituents in abandoned coal-mine discharges, Pennsylvania, USA. Part 2: Geochemical controls on constituent concentrations. *Appl. Geochem.* **23**, 203–226.

Cravotta, III, C. A. and Brady K. B. C. (2015) Priority pollutants and associated constituents in untreated and treated discharges from coal mining or processing facilities in Pennsylvania USA. *Appl. Geochem.* **62**, 108–130.

Czebiniak M. (2016) Pittsburgh Botanic Garden brims with life after abandoned mine cleanup. *Pittsburgh Tribune-Rev.*, October 24, 2016.

Dia A., Gruau G., Olivié-Lauquet G., Riou C., Molénat J. and Curmi P. (2000) The distribution of rare earth elements in groundwaters: Assessing the role of source-rock composition, redox changes and colloidal particles. *Geochim. Cosmochim. Acta* **64**, 4131–4151.

DOE (2011) Critical Materials Strategy. DOE/PI-0009, United States Department of Energy: http://energy.gov/sites/prod/files/DOE_CMS2011_FINAL_Full.pdf.

Dupré B., Viers J., Dandurand J.-L., Polve M., Bénézeth P., Vervier P. and Braun J.-J. (1999) Major and trace elements associated with colloids in organic-rich river waters: ultrafiltration of natural and spiked solutions. *Chem. Geol.* **160**, 63–80.

Edmunds W. E., Skema V. W. and Flint N. K. (1999) Chapter 10. Pennsylvanian. In *The Geology of Pennsylvania* (ed. C. H. Schultz). Pennsylvania Geological Survey and Pittsburgh Geological Society, Harrisburg, pp. 148–169.

Elderfield H., Upstill-Goddard R. and Sholkovitz E. R. (1990) The rare earth elements in rivers, estuaries, and coastal seas and their significance to the composition of ocean waters. *Geochim. Cosmochim. Acta* **54**, 971–991.

European Commission (2014) Report on Critical Raw Materials for the EU.

Franus W., Wiatros-Motyka M. M. and Wdowin M. (2015) Coal fly ash as a resource for rare earth elements. *Environ. Sci. Pollut. Res. Int.* **22**, 9464–9474.

Gammons C. H., Wood S. A., Pedrozo F., Varekamp J. C., Nelson B. J., Shope C. L. and Baffico G. (2005) Hydrogeochemistry and rare earth element behavior in a volcanically acidified watershed in Patagonia, Argentina. *Chem. Geol.* **222**, 249–267.

García M. G., Lecompte K. L., Pasquini A. I., Formica S. M. and Depetris P. J. (2007) Sources of dissolved REE in mountainous streams draining granitic rocks, Sierras Pampeanas (Córdoba, Argentina). *Geochim. Cosmochim. Acta* **71**, 5355–5368.

Genz A., Kornmüller A. and Jekel M. (2004) Advanced phosphorus removal from membrane filtrates by adsorption on activated aluminium oxide and granulated ferric hydroxide. *Wat. Res.* **38**, 3523–3530.

Gimeno Serrano M. J., Auqué Sanz L. F. and Nordstrom D. K. (2000) REE speciation in low-temperature acidic waters and the competitive effects of aluminum. *Chem. Geol.* **165**, 167–180.

Gleason J. D., Patchett P. J., Dickinson W. R. and Ruiz J. (1994) Nd isotopes link Ouachita turbidites to Appalachian sources. *Geology* **22**, 347–350.

Gleason J. D., Patchett P. J., Dickinson W. R. and Ruiz J. (1995) Nd isotopic constraints on sediment sources of the Ouachita-Marathon fold belt. *Geol. Soc. Am. Bull.* **107**, 1192–1210.

Grawunder A., Merten D. and Büchel G. (2014) Origin of middle rare earth element enrichment in acid mine drainage-impacted areas. *Environ. Sci. Pollut. Res.* **21**, 6812–6823.

Gromet L. P., Dymek R. F., Haskin L. A. and Korotev R. L. (1984) The "North American shale composite": Its compilation, major and trace element characteristics. *Geochim. Cosmochim. Acta* **48**, 2469–2482.

Hannigan R. E. and Sholkovitz E. R. (2001) The development of middle rare earth element enrichments in freshwaters: weathering of phosphate minerals. *Chem. Geol.* **175**, 495–508.

Hedin B. C., Capo R. C., Stewart B. W., Hedin R. S., Lopano C. L. and Stuckman M. Y. (2019) The evaluation of critical rare earth element (REE) enriched treatment solids from coal mine drainage passive treatment systems. *Int. J. Coal Geol.* **208**, 54–64.

Hindshaw R. S., Aciego S. M., Piotrowski A. M. and Tipper E. T. (2018) Decoupling of dissolved and bedrock neodymium isotopes during sedimentary cycling. *Geochem. Persp. Lett.*, 43–46.

Hobba, Jr., W. A. (1993) Effects of underground mining and mine collapse on the hydrology of selected basins in West Virginia. *U.S Geol. Surv. Water-Supply Paper* **2384**, 1–79.

Hongshao Z. and Stanforth R. (2001) Competitive adsorption of phosphate and arsenate on goethite. *Environ. Sci. Technol.* **35**, 4753–4757.

Hoyle J., Elderfield H., Gledhill A. and Greaves M. (1984) The behaviour of the rare earth elements during mixing of river and sea waters. *Geochim. Cosmochim. Acta* **48**, 143–149.

Ingri J., Widerlund A., Land M., Gustafsson Ö., Andersson P. and Öhlander B. (2000) Temporal variations in the fractionation of the rare earth elements in a boreal river; the role of colloidal particles. *Chem. Geol.* **166**, 23–45.

Iwashita M., Saito A., Aral M., Furusho Y. and Shimamura T. (2011) Determination of rare earth elements in rainwater collected in suburban Tokyo. *Geochem. J.* **45**, 187–197.

Jacobsen S. B. and Wasserburg G. J. (1980) Sm-Nd isotopic evolution of chondrites. *Earth Planet. Sci. Lett.* **50**, 139–155.

Jennings S. R., Neuman D. R. and Blicker P. S. (2008) *Acid Mine Drainage and Effects on Fish Health and Ecology: A Review*. Reclamation Research Group Publication, Bozeman, MT.

Johannesson K. H., Lyons W. B., Yelken M. A., Gaudette H. E. and Stetzenbach K. J. (1996) Geochemistry of the rare-earth elements in hypersaline and dilute acidic natural terrestrial waters: Complexation behavior and middle rare-earth element enrichments. *Chem. Geol.* **133**, 125–144.

Johannesson K. H. and Zhou X. (1999) Origin of middle rare earth element enrichments in acid waters of a Canadian High Arctic lake. *Geochim. Cosmochim. Acta* **63**, 153–165.

Johnson D. B. and Hallberg K. B. (2005) Acid mine drainage remediation options: a review. *Sci. Tot. Env.* **338**, 3–14.

Joosu L., Lepland A., Kreitsmann T., Üpraus K., Roberts N. M. W., Paiste P., Martin A. P. and Kirsimäe K. (2016) Petrography and the REE-composition of apatite in the Paleoproterozoic Pilgujärvi Sedimentary Formation, Pechenga Greenstone Belt, Russia. *Geochim. Cosmochim. Acta* **186**, 135–153.

Kanazawa Y. and Kamitani M. (2006) Rare earth minerals and resources in the world. *J. Alloys Comp.* **408–412**, 1339–1343.

Kendorski F. S. (2006) Effect of full-extraction undergound mining on ground and surface waters: A 25-year retrospective. In *25th International Conference on Ground Control in Mining, WV*, pp. 425–430.

Kidder D. L. and Eddy-Dilek C. A. (1994) Rare-earth element variation in phosphate nodules from midcontinent Pennsylvanian cyclothems. *J. Sed. Res.* **A64**, 584–592.

Kidder D. L., Krishnaswamy R. and Mapes R. H. (2003) Elemental mobility in phosphatic shales during concretion growth and implications for provenance analysis. *Chem. Geol.* **198**, 335–353.

Lebold J. G. and Kammer T. W. (2006) Gradient analysis of faunal distributions associated with rapid transgression and low accommodation space in a Late Pennsylvanian marine embay-

ment: Biofacies of the Ames Member (Glenshaw Formation, Conemaugh Group) in the northern Appalachian Basin USA. *Palaeogeog. Palaeoclimatol. Palaeoecol.* **231**, 291–314.

Ler A. and Stanforth R. (2003) Evidence for surface precipitation of phosphate on goethite. *Environ. Sci. Technol.* **37**, 2694–2700.

Lev S. M. and Filer J. K. (2004) Assessing the impact of black shale processes on REE and the U-Pb isotope system in the southern Appalachian Basin. *Chem. Geol.* **206**, 393–406.

Leybourne M. I., Goodfellow W. D., Boyle D. R. and Hall G. M. (2000) Rapid development of negative Ce anomalies in surface waters and contrasting REE patterns in groundwaters associated with Zn±Pb massive sulphide deposits. *Appl. Geochem.* **15**, 695–723.

Leybourne M. L. and Cousens B. L. (2005) Rare earth elements (REE) and Nd and Sr isotopes in groundwater and suspended sediments from the Bathurst Mining Camp, New Brunswick: Water-rock reactions and elemental fractionation. In *Rare Earth Elements in Groundwater Flow Systems* (ed. K. H. Johannesson). Springer, Dordrecht, pp. 253–293.

Li S.-L., Calmels D., Han G., Gaillardet J. and Liu C.-Q. (2008) Sulfuric acid as an agent of carbonate weathering constrained by δ^{13}CDIC: Examples from Southwest China. *Earth Planet. Sci. Lett.* **270**, 189–199.

Mao M., Rukhlov A. S., Rowins S. M., Spence J. and Googan L. A. (2016) Apatite trace element compositions: A robust new tool for mineral exploration. *Econ. Geol.* **111**, 1187–1222.

McLennan S. M. (1989) Rare earth elements in sedimentary rocks: Influence of provenance and sedimentary processes. In *Geochemistry and Mineralogy of Rare Earth Elements* (eds. B. R. Lipin and G. A. McKay). Mineralogical Society of America, Chelsea, Michigan, pp. 169–200.

Merten D., Geletneky J., Bergmann H., Haferburg G., Kothe E. and Büchel G. (2005) Rare earth element patterns: A tool for understanding processes in remediation of acid mine drainage. *Chem. Erde* **65**, 97–114.

Möller P. and Bau M. (1993) Rare-earth patterns with positive cerium anomaly in alkaline waters from Lake Van, Turkey. *Earth Planet. Sci. Lett.* **117**, 671–676.

Nordstrom D. K. (2011) Hydrogeochemical processes governing the origin, transport and fate of major and trace elements from mine wastes and mineralized rock to surface waters. *Appl. Geochem.* **26**, 1777–1791.

Nordstrom D. K. and Alpers C. N. (1999) Geochemistry of acid mine waters. In *The Environmental Geochemistry of Mineral Deposits* (eds. G. S. Plumlee and M. J. Logsdon). Society of Economic Geologists, Littleton, CO, pp. 133–160.

Nordstrom D. K., Blowes D. W. and Ptacek C. J. (2015) Hydrogeochemistry and microbiology of mine drainage: An update. *Appl. Geochem.* **57**, 3–16.

Olías M., Cerón J. C., Fernández I. and De la Rosa J. (2005) Distribution of rare earth elements in an alluvial aquifer affected by acid mine drainage: the Guadiamar aquifer (SW Spain). *Environ. Pollut.* **135**, 53–64.

Patchett P. J., Ross G. M. and Gleason J. D. (1999) Continental drainage in North America during the Phanerozoic from Nd isotopes. *Science* **283**, 671–673.

Pérez-López R., Delgado J., Nieto J. M. and Márquez-García B. (2010) Rare earth element geochemistry of sulphide weathering in the São Domingos mine area (Iberian Pyrite Belt): A proxy for fluid–rock interaction and ancient mining pollution. *Chem. Geol.* **276**, 29–40.

Phan T. T., Capo R. C., Stewart B. W., Graney J. R., Johnson J. D., Sharma S. and Toro J. (2015) Trace metal distribution and mobility in drill cuttings and produced waters from Marcellus shale gas extraction: uranium, arsenic, barium. *Appl. Geochem.* **60**, 89–103.

Phan T. T., Gardiner J. B., Capo R. C. and Stewart B. W. (2018a) Geochemical and multi-isotopic (^{87}Sr/^{86}Sr, ^{143}Nd/^{144}Nd, ^{238}U/^{235}U) perspectives of sediment sources, depositional conditions, and diagenesis of the Marcellus Shale, Appalachian Basin, USA. *Geochim. Cosmochim. Acta* **222**, 187–211.

Phan T. T., Hakala J. A. and Bain D. J. (2018b) Influence of colloids on metal concentrations and radiogenic strontium isotopes in groundwater and oil and gas-produced waters. *Appl. Geochem.* **95**, 85–96.

Phan T. T., Hakala J. A., Lopano C. L. and Sharma S. (2019) Rare earth elements and radiogenic strontium isotopes in carbonate minerals reveal diagenetic influence in shales and limestones in the Appalachian Basin. *Chem. Geol.* **509**, 194–212.

Pin C. and Zalduegui J. F. S. (1997) Sequential separation of light rare-earth elements, thorium and uranium by miniaturized extraction chromatography: Application to isotopic analyses of silicate rocks. *Analyt. Chim. Acta* **339**, 79–89.

Plumlee G. S., Smith K. S., Montour M. R., Ficklin W. H. and Mosier E. L. (1999) Geologic controls on the composition of natural waters and mine waters draining diverse mineral-deposit types. In *The Environmental Geochemistry of Mineral Deposits* (eds. G. S. Plumlee and M. J. Logsdon). Society of Economic Geologists, Littleton, CO, pp. 373–433.

Reed J. S., Eriksson K. A. and Kowalewski M. (2005a) Climatic, depositional and burial controls on diagenesis of Appalachian Carboniferous sandstones: qualitative and quantitative methods. *Sed. Geol.* **176**, 225–246.

Reed J. S., Spotila J. A., Eriksson K. A. and Bodnar R. J. (2005b) Burial and exhumation history of Pennsylvanian strata, central Appalachian basin: an integrated study. *Basin Res.* **17**, 259–268.

Ruppert L. F., Kirschbaum M., Warwick P. D., Flores R. M., Affolter R. H. and Hatch J. R. (2002) The US Geological Survey's national coal resource assessment: the results. *Int. J. Coal Geol.* **50**, 247–274.

Sahoo P. K., Tripathy S., Equeenuddin S. M. and Panigrahi M. K. (2012) Geochemical characteristics of coal mine discharge vis-à-vis behavior of rare earth elements at Jaintia Hills coalfield, northeastern India. *J. Geochem. Explor.* **112**, 235–243.

Schatzel S. J. and Stewart B. W. (2003) Rare earth element sources and modification in the Lower Kittanning coal bed, Pennsylvania: implications for the origin of coal mineral matter and rare earth element exposure in underground mines. *Int. J. Coal Geol.* **54**, 223–251.

Schatzel S. J. and Stewart B. W. (2012) A provenance study of mineral matter in coal from Appalachian Basin coal mining regions and implications regarding the respirable health of underground coal workers: A geochemical and Nd isotope investigation. *Int. J. Coal Geol.* **94**, 123–136.

Seredin V. V. and Dai S. (2012) Coal deposits as potential alternative sources for lanthanides and yttrium. *Int. J. Coal Geol.* **94**, 67–93.

Sharma S., Sack A., Adams J. P., Vesper D. J., Capo R. C., Hartsock A. and Edenborn H. M. (2013) Isotopic evidence of enhanced carbonate dissolution at a coal mine drainage site in Allegheny County, Pennsylvania, USA. *Appl. Geochem.* **29**, 32–42.

Sholkovitz E. R. (1992) Chemical evolution of rare earth elements: fractionation between colloidal and solution phases of filtered river water. *Earth Planet. Sci. Lett.* **114**, 77–84.

Sholkovitz E. R. (1995) The aquatic chemistry of rare earth elements in rivers and estuaries. *Aquatic Geochem.* **1**, 1–34.

Sholkovitz E. R., Church T. M. and Arimoto R. (1993) Rare earth element composition of precipitation, precipitation particles, and aerosols. *J. Geophys. Res. Atmos.* **98**, 20587–20599.

Simate G. S. and Ndlovu S. (2014) Acid mine drainage: Challenges and opportunities. *J. Env. Chem. Eng.* **2**, 1785–1803.

Singh M. M. and Kendorski F. S. (1981) Strata disturbance prediction for mining beneath surface water and waste impoundments. 1st International Conference on Ground Control in Mining, Morgantown, WV.

Stewart B. W., Capo R. C. and Chadwick O. A. (1998) Quantitative strontium isotope models for weathering, pedogenesis and biogeochemical cycling. *Geoderma* **82**, 173–195.

Stewart B. W., Capo R. C. and Chadwick O. A. (2001) Effects of rainfall on weathering rate, base cation provenance, and Sr isotope composition of Hawaiian soils. *Geochim. Cosmochim. Acta* **65**, 1087–1099.

Stewart B. W., Capo R. C., Hedin B. C. and Hedin R. S. (2017) Rare earth element resources in coal mine drainage and treatment precipitates in the Appalachian Basin, USA. *Int. J. Coal Geol.* **169**, 28–39.

Stewart B. W., Chapman E. C., Capo R. C., Johnson J. D., Graney J. R., Kirby C. S. and Schroeder K. T. (2015) Origin of brines, salts and carbonate from shales of the Marcellus Formation: Evidence from geochemical and Sr isotope study of sequentially extracted fluids. *Appl. Geochem.* **60**, 78–88.

Sun H., Zhao F., Zhang M. and Li J. (2012) Behavior of rare earth elements in acid coal mine drainage in Shanxi Province, China. *Environ. Earth Sci.* **67**, 205–213.

Tang J. and Johannesson K. H. (2003) Speciation of rare earth elements in natural terrestrial waters: Assessing the role of dissolved organic matter from the modeling approach. *Geochim. Cosmochim. Acta* **67**, 2321–2339.

Trotter J. A., Barnes C. R. and McCracken A. D. (2016) Rare earth elements in conodont apatite: Seawater or pore-water signatures? *Palaeogeog. Palaeoclimatol. Palaeoecol.* **462**, 92–100.

(2010) Coal-Mine-Drainage Projects in Pennsylvania. United States Geological Survey, https://pa.water.usgs.gov/projects/energy/amd/.

Van Gosen B. S., Verplanck P. L., Seal, II, R. R., Long K. R. and Gambogi J. (2017) Rare-earth elements: Chapter O of Critical Mineral Resoures of the United States–Economic and Environmental Geology and Prospects for Future Supply. *U.S. Geol. Surv. Prof. Paper 1802-O, O1-O31*.

Vass C. R., Noble A. and Ziemkiewicz P. F. (2019) The occurrence and concentration of rare earth elements in acid mine drainage and treatment by-products: Part 1—Initial survey of the northern Appalachian Coal Basin. *Min. Metall. Explor.* **36**, 903–916.

Verplanck P. L., Nordstrom D. K., Taylor H. E. and Kimball B. A. (2004) Rare earth element partitioning between hydrous ferric oxides and acid mine water during iron oxidation. *Appl. Geochem.* **19**, 1339–1354.

Wall A. J., Capo R. C., Stewart B. W., Phan T. T., Jain J. C., Hakala J. A. and Guthrie G. D. (2013) High throughput method for Sr extraction from variable matrix waters and $^{87}Sr/^{86}Sr$ isotope analysis by MC-ICP-MS. *J. Anal. At. Spectrom.* **28**, 1338–1344.

Wall F. (2014). In *Rare earth elements*. Critical Metals Handbook. John Wiley & Sons Ltd, pp. 312–339.

Wang G. and Carr T. R. (2013) Organic-rick Marcellus Shale lithofacies modeling and distribution pattern analysis in the Appalachian Basin. *AAPG Bull.* **97**, 2173–2205.

Wasserburg G. J., Jacobsen S. B., DePaolo D. J., McCulloch M. T. and Wen T. (1981) Precise determination of Sm/Nd ratios, Sm and Nd isotopic abundances in standard solutions. *Geochim. Cosmochim. Acta* **45**, 2311–2323.

Welch S. A., Christy A. G., Isaacson L. and Kirste D. (2009) Mineralogical control of rare earth elements in acid sulfate soils. *Geochim. Cosmochim. Acta* **73**, 44–64.

Winters W. R. and Capo R. C. (2004) Groundwater flow parameterization of an Appalachian coal mine complex. *Ground Water* **42**, 700–710.

Wood S. A., Shannon W. M. and Baker L. (2005) The aqueous geochemistry of the rare earth elements and yttrium. Part 13: REE geochemistry of mine drainage from the Pine Creek area, Coeur d'Alene River valley, Idaho, USA. In *Rare Earth Elements in Groundwater Flow Systems* (ed. K. H. Johannesson). Springer, Dordrecht, pp. 89–110.

Worrall F. and Pearson D. G. (2001) The development of acidic groundwaters in coal-bearing strata: Part I. Rare earth element fingerprinting. *Appl. Geochem.* **16**, 1465–1480.

Yang J., Torres M., McManus J., Algeo T. J., Hakala J. A. and Verba C. (2017) Controls on rare earth element distributions in ancient organic-rich sedimentary sequences: Role of post-depositional diagenesis of phosphorus phases. *Chem. Geol.* **466**, 533–544.

Younger P. L. (1997) The longevity of minewater pollution: a basis for decision-making. *Sci. Total Environ.* **194**(195), 457–466.

Zhang C., Wang L. and Zhang S. (1998) Geochemistry of rare earth elements in the mainstream of the Yangtze River, China. *Appl. Geochem.* **13**, 451–462.

Zhang L., Algeo T. J., Cao L., Zhao L., Chen Z.-Q. and Li Z. (2016) Diagenetic uptake of rare earth elements by conodont apatite. *Palaeogeog. Palaeoclimatol. Palaeoecol.* **458**, 176–197.

Zhang W. and Honaker R. Q. (2018) Rare earth elements recovery using staged precipitation from a leachate generated from coarse coal refuse. *Int. J. Coal Geol.* **195**, 189–199.

Zhao F., Cong Z., Sun H. and Ren D. (2007) The geochemistry of rare earth elements (REE) in acid mine drainage from the Sitai coal mine, Shanxi Province, North China. *Int. J. Coal Geol.* **70**, 184–192.

Ziemkiewicz P., He T., Noble A. and Liu X. (2016) Recovery of rare earth elements (REEs) from coal mine drainage. In *Proc. 37th W. Virginia Surface Mine Drainage Task Force Symposium*, pp. 43–50.

Associate editor: Jeffrey G. Catalano